Article

Geochronology and Geochemistry of Archean TTG and Tremolite Schist Xenoliths in Yemadong Complex: Evidence for Mesoarchean Continental Crustal evolution in Kongling High-grade Metamorphic Terrane, Yangtze Craton, China

Wenxiao Zhou[1*], Yunxu Wei[2*], Zhengxiang Hu[3], Haiquan Li[1], Xianxiao Huang[1,4] and Xiaoming Zhao[2]

[1] Institute of geological survey, China University of Geosciences, Wuhan 430074, China
[2] Wuhan Institute of Geology and Minerals Resources, Wuhan Center of Geological Survey, Wuhan, 430205, China
[3] Hubei Geological Survey, Wuhan, 430205, China
[4] Guangxi Regional Geological Survey, Guilin, 541001, China
* Correspondence: zhouwenxiao@cug.edu.cn; Tel.: +86 18607142327

Abstract: The origin and significance of the tonalite–trondhjemite–granodiorite (TTG) units and the familiar metabasite xenoliths they host in the Yangtze Craton, China, remain controversial, and resolving these issues is important if we are to understand the evolution of the early Yangtze Craton. We focused on biotite–tremolite schist xenoliths in the Archean TTG units of the Kongling high-grade metamorphic terrane, and U–Pb dating of their zircons yielded $^{207}Pb/^{206}Pb$ ages of ca. 3.00 Ga, which provides a minimum age for the formation of the pre-metamorphic basic igneous rock. The host TTGs and late intrusive granitic dikes yield three groups of upper intercept ages at 2.87–2.88, 2.91–2.94, and 3.07 Ga, and a concordant age at 2.94 Ga, which suggest that the Yangtze continental nucleus underwent three important metamorphic–magmatic events in the Mesoarchean at ca. 3.00, 2.94, and 2.87 Ga. The biotite–tremolite schists have high ratios of K_2O/Na_2O and high contents of CaO, Cr, and Ni, thus showing the characteristics of high-K calc-alkaline island-arc volcanic rocks (basalt–andesite) that form by the partial melting of subducted oceanic crust. The data also provide further proof that a Mesoarchean metamorphic basement exists in the Yangtze Plate. Derivation of the magmatic protoliths of the biotite–tremolite schist enclaves from an oceanic crust during slab subduction, and the presence of these xenoliths within the TTG suite, indicate the existence of the initiation of plate tectonics during the Mesoarchean (≤2.94 Ga). The dikes of alkali granite might also be related to this oceanic plate subduction.

Keywords: Archean TTG; Tremolite Schist; Yemadong Complex; Kongling High-grade Metamorphic Terrane; Yangtze Craton

1. Introduction

The two largest cratons in China, the South China Block (SCB) and the North China Craton (NCC), collided along the Qinling–Dabie–Sulu orogenic belt in the Triassic or earlier [1, 2]. However, Archean rocks are relatively scarce in the SCB [3] compared with the NCC where they are widely present [4-6]. The Kongling high-grade metamorphic terrane (KHMT) is the nucleus of the Yangtze Block, and one of just a few Archean terranes reported so far in the SCB [7-11]. Various ages for these rocks have been obtained during previous geochronological studies, especially for the TTG gneisses in the KHMT [7-10, 12], but it is generally accepted that the peak period of TTG magmatism occurred at 2.90–2.85 Ga, and magmatic rocks older than 3.0 Ga are relatively rare [7, 9, 13, 14]. Previous studies

of these Archean crustal rocks in the SCB have been limited, producing just a few isolated geochemical or geochronological data [7-9, 11, 13, 15-17]. Outcrops of Neoarchean and Mesoarchean rocks have not been directly identified in the field in the Yangtze Craton, and whether or not even more ancient rocks exist in the Yangtze Craton is a problem yet to be solved. In the absence of clear evidence from rocks in the field, the main stages of formation of the KHMT have been unclear, and this also means that issues about the early formation and evolution of the nucleus of the Yangtze Craton have remained controversial.

In this paper, we provide details of the whole-rock geochemistry, zircon U–Pb geochronology, and Lu–Hf isotope compositions of five intertwined samples from one outcrop at Shuiyuesi in the North Kongling Terrane of the Yangtze Craton. Our results show that the protolith of the biotite–tremolite schist enclaves in the TTG gneisses was a calc-alkaline basaltic andesite, and the U–Pb and Lu–Hf data reveal that the magma was emplaced at ca. 3.00 Ga. Taking into account previously published data, our new data show that the biotite–tremolite schists and the host 3.00–2.90 Ga TTG gneisses constitute a Mesoarchean granite–greenstone belt in the Yangtze Craton, which provides clear evidence for the existence of Archean continental crust and plate tectonics during the development of the craton. In addition, data for the dikes of alkali granite suggest subduction of oceanic crust took place at 2.94–2.87 Ga in the north Yangtze Craton, and this might also be related to the same early period of oceanic plate subduction that records the initiation of plate-tectonic mechanisms in the Mesoarchean from 2.94 Ga at the latest.

2. Geological background and sample descriptions

2.1. Geological background

The SCB was formed by the Grenvillian continental collision [18] of the Yangtze Craton and the Cathaysia Block. The Yangtze Craton is bounded to the west by the Songpan–Ganzi Block, to the north by the Qinling–Dabie–Sulu Orogen, and to the south by the Jiangnan Orogen (Figure 1a). The Kongling Terrane is in the northeastern part of the Yangtze Craton, has an oval dome structure, and covers an area of ~360 km^2 (Figure 1b). It is divided by the Wuduhe Fault into two segments known as the North Kongling Terrane, dominated by Archean TTG granitic gneisses and metasedimentary rocks (Figure 1c)[7, 19], and the South Kongling Terrane, dominated by Neoproterozoic TTG intrusions such as the Huangling Dome [20-22]. Previous studies have revealed three major episodes of Archean crustal growth in the Kongling Terrane at 3.3–3.2, 2.9–2.8, and 2.7–2.6 Ga [7-9, 15, 19, 23]. The 3.3–3.2 Ga TTG gneisses and migmatites are preserved locally in the widespread 2.9–2.8 Ga TTG rocks [7, 8, 19, 23], and the 2.7–2.6 Ga A-type granitic gneisses, discovered recently in the eastern North Kongling Terrane, mark the termination of the subduction-related TTG magmatism and the addition of significant juvenile crustal components [15]. Crustal materials as old as 3.8 Ga have only been inferred from zircon Hf model ages [7, 8], and although one 3.8 Ga detrital zircon has been reported in the Kongling Terrane from a Neoproterozoic sandstone [10], its source is uncertain.

Preprints (www.preprints.org) | NOT PEER-REVIEWED | Posted: 8 October 2019 doi:10.20944/preprints201910.0075.v1

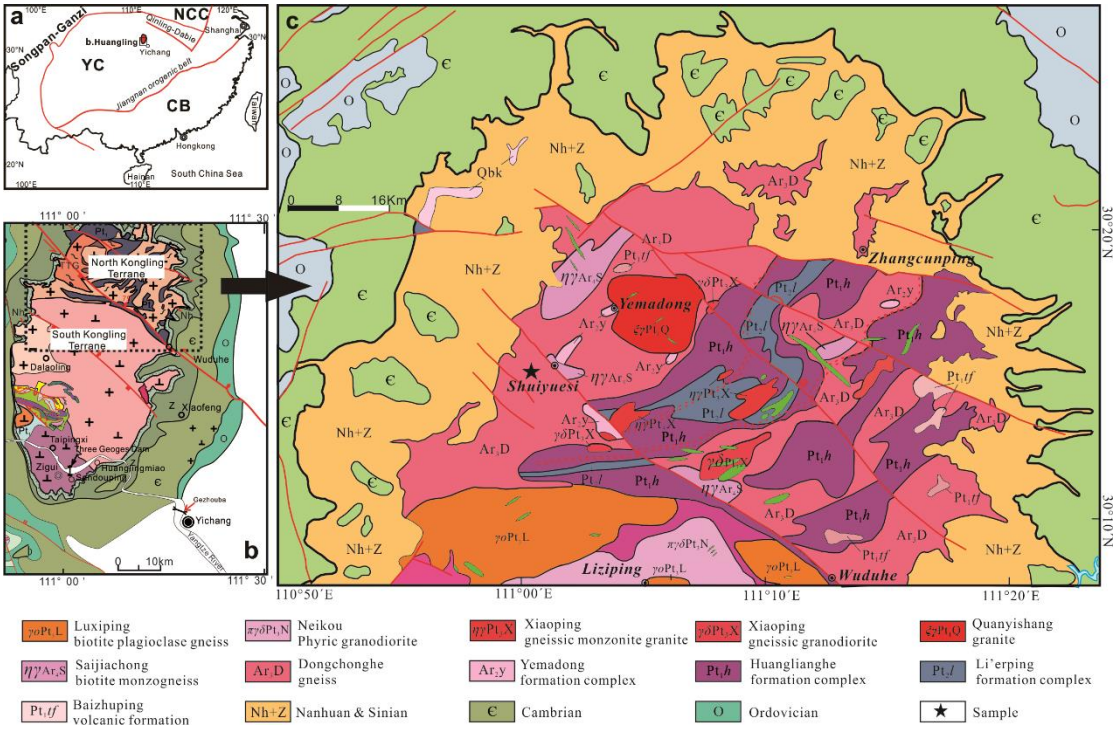

Figure 1. Geological map of the Archean Kongling Terrane (modified from Gao et al., 2011). (a) Major tectonic divisions of South China. NCC denotes the North China Craton, YC denotes the Yangtze Craton, and CB denotes the Cathaysia Block. (b) Structure and division of the Kongling Terrane. (c) Geological map of the North Kongling Terrane. Star denotes the sample location.

2.2. Sampling

Samples D0002-1 (biotite–tremolite schist), D0002-2 (tonalitic gneiss), D0002-3 (trondhjemitic gneiss), D0002-5 (granitic gneiss), and KH110 (granitic gneiss) are fresh rock samples that were taken from a fracture surface (Figure 2a) near the Xiafangxi River (31°08′25″ N, 111°00′04″ E) in the North Kongling Terrane, and we also collected one sample of fresh granitic gneiss (D0002-4) from Shuiyuesi village (on the other side of the river at 31°08′24″ N, 111°00′05″ E) (Figure 1c). Samples SMK-1 (trondhjemitic gneiss) and SMK-4 (trondhjemitic gneiss) were collected from Shimenkou to the northwest of Wuduhe town near a streamlet (31°10′11″N, 111°11′22″E). The exposed lithologies are mainly gray gneisses that are strongly foliated and locally migmatized with quartzofeldspathic bands and thin biotite-rich layers. The biotite–tremolite schist sample comes from an inclusion in the TTG gneiss (Figure 2a,d), and the granitic gneisses at this location form sheet-like intrusions that cut across the other TTG gneisses (Figure 2e,f). The data for other samples such as PM51-6-1, PM51-6-2, PM51-6-3, D050-1, and D050-2, included on some of the later figures, are from the unpublished data of Yunxu Wei.

Preprints (www.preprints.org) | NOT PEER-REVIEWED | Posted: 8 October 2019 doi:10.20944/preprints201910.0075.v1

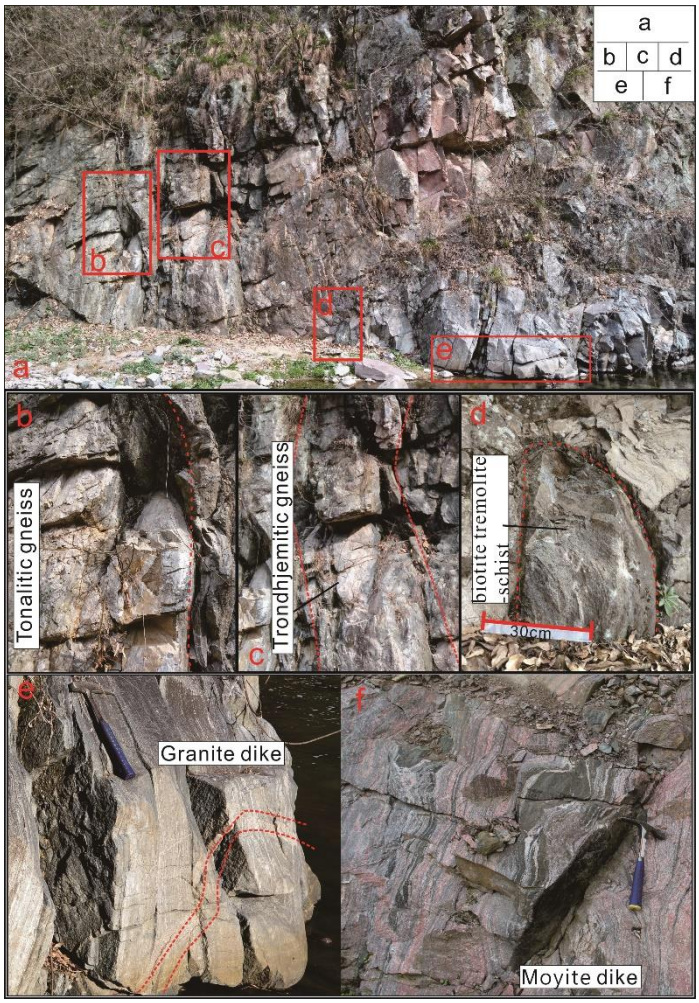

Figure 2. Field photographs of the Shuiyuesi granite–greenstone terrane showing outcrops of (a) the Taoyuan trondhjemite gneiss, (b) the tonalitic gneiss, (c) the trondhjemitic gneiss, (d) the biotite–tremolite schist, (e) a granite dike, and (f) the moyite dike.

2.2.1. TTG

The TTG samples are medium- to fine-grained, gneissose, and composed mainly of plagioclase, quartz, K-feldspar, and biotite. The plagioclase content is 60%–70%, polysynthetic twinning is visible, and the crystals show obvious K-metasomatism with visible reaction rims of K-feldspar. Most surfaces of the plagioclase are pitted with sericite and biotite alteration. Anhedral quartz makes up 10%–15% of TTG rocks, and it forms irregular aggregates of granular grains in the size range of 0.2–0.8 mm. The platy biotite that makes up 5%–10% of the rock occurs as dispersed grains that have been altered to muscovite and sericite. Less abundant K-feldspar and other minerals, such as epidote, are also present (Figure 3a,b).

2.2.2. granite dikes

The granite dikes are made up of plagioclase, quartz, K-feldspar, and lesser amounts of biotite. The K-feldspar is anhedral and granular, and shows cross-hatched twinning. Sample D0002-5 underwent K-feldspathization and has a high K-feldspar content of 70%. Small amounts of epidote are also present (Figure3c).

Preprints (www.preprints.org) | NOT PEER-REVIEWED | Posted: 8 October 2019 doi:10.20944/preprints201910.0075.v1

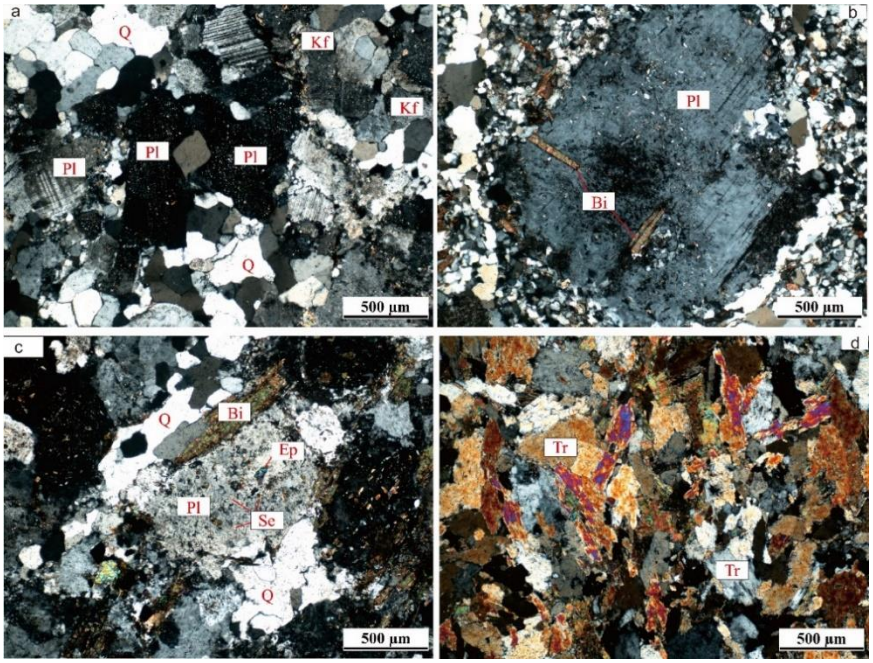

Figure 3. Photomicrographs of the TTG gneiss and biotite–tremolite schist in the Northern Kongling Terrane. (a): Sample D0002-2; (b): Sample SMK-1; (c): Sample D0002-4; (d): Sample D0002-1.

2.2.3. biotite–tremolite schist

The biotite–tremolite schist has a crystalloblastic texture and schistose structure, with biotite (Bi) and tremolite (Tr) as the main minerals, along with some dolomite and magnetite. The tremolite is euhedral, columnar, and colorless, and the long axes of the crystals show a preferred orientation (Figure 3d). The tremolite grains are 0.2–2.0 mm in size and make up 60%–65% of the rock. The 0.2–2.0 mm grains of biotite are euhedral, platy, and yellowish green, and they display a preferred orientation (Figure 3d). The biotite makes up about 30%–35% of the rock. The 0.1–0.2 mm grains of granular dolomite fill the spaces between the tremolite and biotite. They make up 3%–4% of the rock.

3. Analytical Methods

3.1. Zircon Morphology

Sample processing for zircon separation involved crushing, initial heavy liquid separation and subsequent magnetic separation. Representative zircons were hand-picked and mounted on adhesive tape, embedded in epoxy resin, polished to about half their size and photographed in reflected and transmitted light (Song et al., 2002). CL images were used to reveal the internal structures of zircons and to help select optimum spot locations for later in situ analysis. The imaging was done at the State Key Laboratory of Continental Dynamics, Xi'an and the State Key Laboratory of Geological Processes. The laboratory in Xi'an uses a FEI Quanta 400 FEG high resolution emission field environmental scanning electron microscope connected to an Oxford INCA350 energy dispersive system (EDS) and a Gatan Mono CL3+ system. The working distance for the CL system was 8.4 mm, while the EDS used a spot size of 6.7 nm with a voltage of 10 kV.

3.2. Zircon U–Pb Dating

Laser ablation ICP-MS zircon U–Pb analyses were conducted on an Agilent 7500a ICP-MS equipped with a 193 nm laser, which is housed at the Department of Geology, Northwest University in Xi'an, China. During analysis, the spot diameter was 30 μm. Raw count rates for ^{29}Si, ^{204}Pb, ^{206}Pb, ^{207}Pb, ^{208}Pb, ^{232}Th and ^{238}U were collected for age determination. U, Th and Pb concentrations were calibrated by using ^{29}Si as the internal calibrant and NIST 610 as the reference material. The $^{207}Pb/^{206}Pb$

and $^{206}Pb/^{238}U$ ratios were calculated using the GLITTER program, which were then corrected using the Harvard zircon 91500 as external calibrant. According to the method of Ballard, Palin [24], measured $^{207}Pb/^{206}Pb$, $^{206}Pb/^{238}U$ and $^{208}Pb/^{232}Th$ ratios in zircon 91500 were averaged over the course of the analytical session and used to calculate correction factors. These correction factors were then applied to each sample to correct for both instrumental mass bias and depth-dependent elemental and isotopic fractionation. The detailed analytical technique is described in Yuan, Gao [25]. The ^{204}Pb isotope cannot be precisely measured with this technique, due to a combination of low signal and interference from small amounts of ^{204}Hg in the Ar gas supply. Common Pb contents were therefore evaluated using the method described by Andersen [26]. The age calculations and plotting of concordia diagrams were made using ISOPLOT (ver 3.15)[27]. The errors quoted in tables and figures are at the 2σ levels.

3.3. Major and Trace Element Analyses

Whole-rock samples were crushed in a corundum jaw crusher (to a size of 60 mesh). About 60 g was powdered in an agate ring mill to a size of less than 200 mesh. Major element contents of the samples were determined by X-ray fluorescence analysis of fused glass beads using a spectrometer (3080E1; Rigaku, Tokyo, Japan) and trace elements were determined on the ICP MS (X.series, Thermo Fisher Scientific, Germany) at the Wuhan Rock and Mineral Analysis Center, Ministry of Land and Resources Research, China. Analytical precision and accuracy with these methods are better than 5% for most elements. The ferric–ferrous iron proportions were determined by wet chemistry.

3.4. Zircon Lu–Hf Isotope Analysis

Experiments were conducted using a Neptune Plus MC-ICP MS (Thermo Fisher Scientific, Germany) in combination with a Geolas 2005 ArF-excimer laser ablation system (Lambda Physik, Göttingen, Germany) that was hosted at the state Key Laboratory of Geological Processes and Mineral Resources, China University of Geosciences in Wuhan. The energy density of laser ablation used in this study was 5.3 J/cm^2. A 'wire' signal smoothing device is included in this laser ablation system, ensuring the production of smooth signals at even very low laser repetition rates down to 1Hz [28, 29]. Detailed operating conditions for the laser ablation system and the MC-ICP MS instrument, along with the analytical methods, are described in Hu, Liu [28].

4. Results

4.1. Zircon U–Pb ages

4.1.1. Biotite tremolite schist

The zircon grains from the biotite–tremolite schist (D0002-1) are subhedral to anhedral and can be classified into two types based on their CL images. Most grains show oscillatory zoning typical of magmatic zircons. The other zircon grains (red circles) display obvious metamorphic core structures (Figure 4).

Preprints (www.preprints.org) | NOT PEER-REVIEWED | Posted: 8 October 2019 doi:10.20944/preprints201910.0075.v1

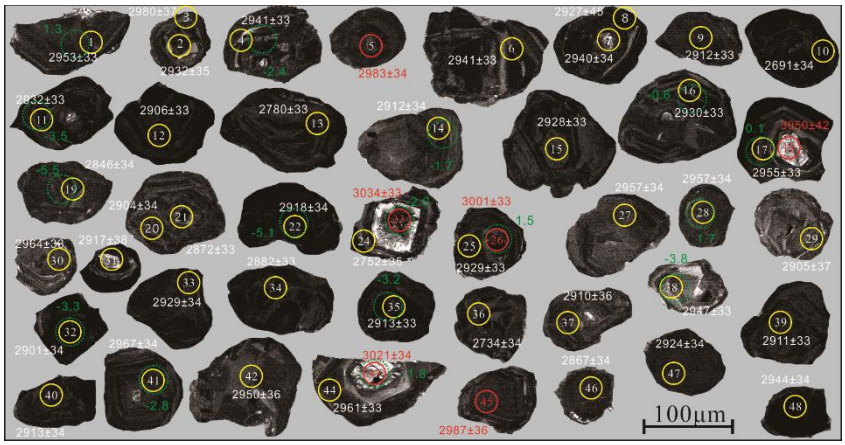

Figure 4. Representative cathodoluminescence images of zircons from the biotite–tremolite schist (D0002-1). The yellow circles show the locations of the LA–ICP–MS U–Pb analyses. The white number in each circle is the number of the analysis. The white number outside each circle is the age (Ma) for each site. The red circles and numbers give the analysis numbers and ages (Ma) for the smaller relict cores in those complex zircons.

Forty-eight spots on 41 grains were analyzed (Figure 4), and 13 of the U–Pb isotopic data are discordant (Figure 5a), suggesting Pb loss caused by a later metamorphic event. These analyses, combined with six concordant spots, form a discordia line that yields an upper intercept $^{207}Pb/^{206}Pb$ age of 2994 ± 26 Ma (2σ, MSWD = 6.1, n = 19). The six concordant spots yield a weighted mean $^{207}Pb/^{206}Pb$ age of 3011 ± 27 Ma (2σ, MSWD = 2.1, n = 6). The remaining 29 spots with ages of 2967–2901 Ma fall close to the upper intercept, are nearly concordant (concordance >98%), and give a weighted mean $^{207}Pb/^{206}Pb$ age of 2933 ± 13 Ma (2σ, MSWD = 0.34, n = 29).

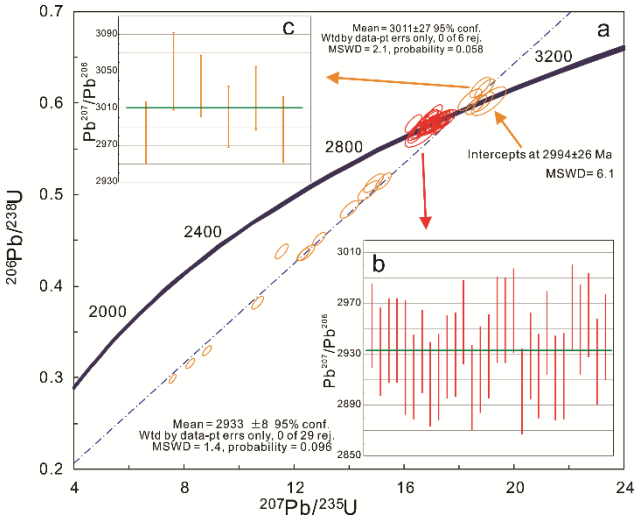

Figure 5. Zircon U–Pb age diagrams for the biotite–tremolite schist (D0002-1). (a) Orange circles for all analyzed spots (n = 19) with a discordia curve that shows an upper intercept age of 2994 ± 26 Ma (MSWD = 6.1). Red circles for a concordia curve (n = 29) yield an age of 2940 ± 19 Ma (MSWD = 0.42). (b) Weighted mean values for all spots with concordant ages (n = 29). The mean age is 2933 ± 8 Ma (MSWD = 1.4). (c) Weighted mean values for six spots that yield a concordant age of 3011 ± 27 Ma (MSWD = 2.1).

202

Table 1 LA-ICP MS U-Pb data for zircons from the Biotite tremolite-schist (D0002-1) in Northern Kongling terrain.

Spots	Pb*(ppm)	Th(ppm)	U(ppm)	Th/U	Isotopic ratio						Age (Ma)					
					$^{207}Pb/^{206}Pb$	1σ	$^{207}Pb/^{235}U$	1σ	$^{206}Pb/^{238}U$	1σ	$^{207}Pb/^{206}Pb$	1σ	$^{207}Pb/^{235}U$	1σ	$^{206}Pb/^{238}U$	1σ
D0002-1-1	268.569	23.96	375.71	0.06	0.21621	0.00452	17.33606	0.21489	0.58140	0.00672	2953	33	2954	12	2955	27
D0002-1-2	124.063	29.63	171.58	0.17	0.21346	0.00464	16.95341	0.23701	0.57588	0.00711	2932	35	2932	13	2932	29
D0002-1-3	221.229	50.82	408.89	0.12	0.20669	0.00481	12.43155	0.20328	0.43612	0.00581	2880	37	2638	15	2333	26
D0002-1-4	313.328	30.52	440.28	0.07	0.21462	0.00449	17.10817	0.21349	0.57799	0.00670	2941	33	2941	12	2941	27
D0002-1-5	*209.109*	*47.03*	*267.19*	*0.18*	*0.22042*	*0.00463*	*18.75618*	*0.23812*	*0.61701*	*0.00724*	*2984*	*33*	*3029*	*12*	*3098*	*29*
D0002-1-6	354.665	23.73	504.1	0.05	0.21463	0.00445	17.03289	0.20545	0.57542	0.00656	2941	33	2937	12	2930	27
D0002-1-7	206.712	110.4	312.03	0.35	0.21448	0.00451	15.22331	0.19163	0.51465	0.00598	2940	34	2829	12	2676	25
D0002-1-8	193.319	18.14	277.57	0.07	0.21286	0.00603	16.65719	0.40356	0.56743	0.01027	2927	45	2915	23	2897	42
D0002-1-9	312.621	62.21	439.62	0.14	0.21086	0.00440	16.61195	0.20437	0.57123	0.00657	2912	33	2913	12	2913	27
D0002-1-10	337.012	78.17	934.45	0.08	0.18419	0.00380	7.58116	0.08899	0.29844	0.00333	2691	34	2183	11	1684	17
D0002-1-11	432.006	32.65	614.04	0.05	0.21349	0.00438	16.94505	0.19711	0.57550	0.00644	2932	33	2932	11	2930	26
D0002-1-12	286.315	71.76	392.29	0.18	0.21013	0.00435	16.89043	0.20278	0.58282	0.00662	2907	33	2929	12	2960	27
D0002-1-13	324.191	70.16	809.89	0.09	0.19438	0.00400	8.82733	0.10344	0.32927	0.00368	2780	33	2320	11	1835	18
D0002-1-14	251.962	18.91	365.09	0.05	0.21084	0.00448	16.46328	0.21471	0.56618	0.00671	2912	34	2904	12	2892	28
D0002-1-15	376.075	53.18	530.62	0.1	0.21293	0.00438	16.88126	0.19790	0.57486	0.00646	2928	33	2928	11	2928	26
D0002-1-16	391.86	33.99	557.26	0.06	0.21314	0.00443	16.87650	0.20515	0.57411	0.00657	2930	33	2928	12	2925	27
D0002-1-17	185.975	18.98	260.3	0.07	0.21657	0.00452	17.33450	0.21425	0.58035	0.00670	2955	33	2954	12	2950	27
D0002-1-18	*91.9233*	*141.26*	*95.18*	*1.48*	*0.22974*	*0.00609*	*19.07141*	*0.41752*	*0.60192*	*0.01027*	*3050*	*42*	*3045*	*21*	*3038*	*41*
D0002-1-19	343.027	64.54	737.85	0.09	0.20238	0.00426	10.65873	0.13367	0.38187	0.00440	2846	34	2494	12	2085	21
D0002-1-20	313.926	26.19	448.06	0.06	0.20976	0.00441	16.61865	0.20965	0.57444	0.00669	2904	34	2913	12	2926	27
D0002-1-21	314.865	37.31	596.23	0.06	0.20567	0.00424	12.32644	0.14497	0.43456	0.00487	2872	33	2630	11	2326	22
D0002-1-22	236.236	59.72	324.54	0.18	0.21161	0.00450	16.96753	0.22310	0.58139	0.00693	2918	34	2933	13	2954	28
D0002-1-23	*173.71*	*337.43*	*157.66*	*2.14*	*0.22747*	*0.00478*	*18.86551*	*0.23840*	*0.60134*	*0.00704*	*3034*	*33*	*3035*	*12*	*3035*	*28*
D0002-1-24	187.438	21.85	352.47	0.06	0.19116	0.00408	11.54202	0.15168	0.43779	0.00515	2752	35	2568	12	2341	23
D0002-1-25	284.156	73.81	394.07	0.19	0.21301	0.00439	16.88046	0.19999	0.57460	0.00648	2929	33	2928	11	2927	27
D0002-1-26	*186.789*	*67.44*	*234.93*	*0.29*	*0.22281*	*0.00465*	*18.91875*	*0.23352*	*0.61565*	*0.00711*	*3001*	*33*	*3038*	*12*	*3093*	*28*
D0002-1-27	197.243	59.85	266.04	0.22	0.21679	0.00462	17.41789	0.22991	0.58253	0.00696	2957	34	2958	13	2959	28
D0002-1-28	270.814	34.35	378.21	0.09	0.21679	0.00458	17.34902	0.22299	0.58025	0.00683	2957	34	2954	12	2950	28
D0002-1-29	204.524	35.65	342.9	0.1	0.20991	0.00479	14.01085	0.22045	0.48396	0.00634	2905	37	2750	15	2545	28

D0002-1-30	233.611	34.72	325.56	0.11	0.21778	0.00455	17.36771	0.21501	0.57822	0.00667	2964	33	2955	12	2942	27
D0002-1-31	173.439	114.24	255.11	0.45	0.21143	0.00509	14.69424	0.26157	0.50390	0.00716	2917	38	2796	17	2631	31
D0002-1-32	401.129	63.14	571.32	0.11	0.20940	0.00445	16.44920	0.21547	0.56955	0.00676	2901	34	2903	13	2906	28
D0002-1-33	206.581	75.09	279.14	0.27	0.21305	0.00454	16.95129	0.22391	0.57689	0.00689	2929	34	2932	13	2936	28
D0002-1-34	375.747	77.15	674.94	0.11	0.20700	0.00429	12.89300	0.15462	0.45159	0.00511	2882	33	2672	11	2402	23
D0002-1-35	327.001	24.51	456.57	0.05	0.21094	0.00439	17.08940	0.20854	0.58739	0.00672	2913	33	2940	12	2979	27
D0002-1-36	418.612	149.17	1087.3	0.14	0.18910	0.00397	8.21635	0.10200	0.31503	0.00359	2734	34	2255	11	1765	18
D0002-1-37	249.133	91.79	382.4	0.24	0.21063	0.00477	14.88239	0.23075	0.51229	0.00667	2910	36	2808	15	2666	28
D0002-1-38	296.541	83.85	405.14	0.21	0.21543	0.00446	17.21920	0.20670	0.57951	0.00658	2947	33	2947	12	2947	27
D0002-1-39	382.046	33.95	537.19	0.06	0.21075	0.00437	16.94361	0.20545	0.58291	0.00665	2911	33	2932	12	2961	27
D0002-1-40	297.652	97.44	415.76	0.23	0.21096	0.00447	16.59041	0.21542	0.57019	0.00673	2913	34	2912	12	2909	28
D0002-1-41	215.451	17.07	301.49	0.06	0.21811	0.00467	17.52299	0.23592	0.58249	0.00704	2967	34	2964	13	2959	29
D0002-1-42	204.544	62.19	278.46	0.22	0.21581	0.00481	17.26824	0.25920	0.58013	0.00747	2950	36	2950	14	2949	30
D0002-1-43	*189.651*	*292.08*	*189.43*	*1.54*	*0.22559*	*0.00481*	*18.61637*	*0.24784*	*0.59832*	*0.00720*	*3021*	*34*	*3022*	*13*	*3023*	*29*
D0002-1-44	223.334	19.86	315.31	0.06	0.21729	0.00451	17.26152	0.20936	0.57596	0.00657	2961	33	2950	12	2932	27
D0002-1-45	*345.736*	*68.26*	*458.09*	*0.15*	*0.22086*	*0.00496*	*18.38280*	*0.28242*	*0.60345*	*0.00791*	*2987*	*36*	*3010*	*15*	*3044*	*32*
D0002-1-46	235.101	36.52	331.31	0.11	0.20501	0.00428	16.32611	0.20154	0.57738	0.00663	2867	34	2896	12	2938	27
D0002-1-47	230.153	59.05	320.01	0.18	0.21243	0.00448	16.82547	0.21542	0.57425	0.00673	2924	34	2925	12	2925	28
D0002-1-48	228.113	114.02	306.79	0.37	0.21499	0.00456	17.10588	0.22324	0.57686	0.00684	2944	34	2941	13	2936	28

203 **Table 2** LA-ICP MS U-Pb data for zircons from the tonalitic gneiss (D0002-2) in Northern Kongling terrain.

Grain no.	Th(ppm)	U(ppm)	Th/U	Pb*(ppm)	Isotopic ratio						Age (Ma)					
D0002-2					$^{207}Pb/^{206}Pb$	1σ	$^{207}Pb/^{235}U$	1σ	$^{206}Pb/^{238}U$	1σ	$^{207}Pb/^{206}Pb$	1σ	$^{207}Pb/^{235}U$	1σ	$^{206}Pb/^{238}U$	1σ
D0002-2-1	71.24	304.34	0.23	162.47	0.20266	0.00442	12.45560	0.16803	0.44539	0.00532	2848	35	2639	13	2375	24
D0002-2-2	134.54	362.85	0.37	262.99	0.21377	0.00467	16.97110	0.23208	0.57536	0.00698	2934	35	2933	13	2930	29
D0002-2-3	83.40	251.27	0.33	122.61	0.20213	0.00462	10.57012	0.16008	0.37902	0.00477	2843	37	2486	14	2072	22
D0002-2-4	99.01	100.17	0.99	79.81	0.22122	0.00503	17.98436	0.27663	0.58925	0.00769	2990	36	2989	15	2986	31
D0002-2-5	45.73	632.32	0.07	338.93	0.20168	0.00435	12.59899	0.16487	0.45282	0.00532	2840	35	2650	12	2408	24

 doi:10.20944/preprints201910.0075.v1

D0002-2-6	48.09	1151.26	0.04	291.99	0.17267	0.00365	5.23377	0.06391	0.21973	0.00248	2584	35	1858	10	1280	13
D0002-2-7	139.19	129.94	1.07	114.25	0.22211	0.00527	18.13740	0.30902	0.59202	0.00826	2996	38	2997	16	2998	33
D0002-2-8	73.40	319.80	0.23	135.60	0.19137	0.00415	8.92462	0.11752	0.33812	0.00394	2754	35	2330	12	1878	19
D0002-2-9	61.45	1394.04	0.04	190.87	0.13729	0.00314	2.27304	0.03359	0.12004	0.00141	2193	39	1204	10	731	8
D0002-2-10	62.86	92.59	0.68	73.46	0.21513	0.00500	17.11077	0.27670	0.57669	0.00772	2945	37	2941	16	2935	32
D0002-2-11	28.51	36.94	0.77	32.96	0.21751	0.00511	18.95927	0.31692	0.63203	0.00870	2962	37	3040	16	3158	34
D0002-2-12	53.24	62.82	0.85	58.78	0.21880	0.00532	19.90844	0.36192	0.65978	0.00969	2972	39	3087	18	3266	38
D0002-2-13	56.85	49.60	1.15	44.46	0.21670	0.00623	17.38446	0.42837	0.58179	0.01066	2956	46	2956	24	2956	43
D0002-2-14	166.78	581.28	0.29	345.30	0.20563	0.00429	13.19568	0.15435	0.46539	0.00513	2871	34	2694	11	2463	23
D0002-2-15	137.38	480.03	0.29	366.94	0.20825	0.00436	17.03959	0.20189	0.59341	0.00659	2892	34	2937	11	3003	27
D0002-2-16	173.94	1122.43	0.15	353.57	0.17636	0.00371	6.20888	0.07442	0.25532	0.00282	2619	35	2006	10	1466	14
D0002-2-17	52.81	147.98	0.36	83.85	0.20247	0.00443	11.96375	0.16267	0.42854	0.00506	2846	35	2602	13	2299	23
D0002-2-18	48.64	1114.59	0.04	240.49	0.15235	0.00335	3.82124	0.05162	0.18190	0.00207	2373	37	1597	11	1077	11
D0002-2-19	148.53	105.15	1.41	99.83	0.21726	0.00484	17.42077	0.25365	0.58154	0.00725	2961	36	2958	14	2955	30
D0002-2-20	93.76	110.01	0.85	95.03	0.21602	0.00503	17.28566	0.28212	0.58034	0.00779	2951	37	2951	16	2950	32
D0002-2-21	164.07	106.66	1.54	104.72	0.21552	0.00500	17.22010	0.27903	0.57949	0.00773	2948	37	2947	16	2947	32
D0002-2-22	91.43	408.62	0.22	314.45	0.20822	0.00434	17.02669	0.19973	0.59306	0.00652	2892	33	2936	11	3002	26
D0002-2-23	58.32	64.51	0.90	56.60	0.21608	0.00524	17.31438	0.31020	0.58115	0.00831	2952	39	2952	17	2953	34
D0002-2-24	109.25	749.04	0.15	337.80	0.19974	0.00414	9.84360	0.11264	0.35741	0.00386	2824	33	2420	11	1970	18
D0002-2-25	78.10	110.40	0.71	94.40	0.21471	0.00470	17.20817	0.23821	0.58121	0.00699	2941	35	2947	13	2954	28

D0002-2-26	66.19	292.10	0.23	235.85	0.22759	0.00477	18.87061	0.22583	0.60128	0.00666	3035	33	3035	12	3035	27
D0002-2-27	58.03	101.61	0.57	84.68	0.21038	0.00470	16.99404	0.24982	0.58577	0.00729	2909	36	2935	14	2972	30
D0002-2-28	265.37	652.99	0.41	462.17	0.20551	0.00426	14.54951	0.16672	0.51339	0.00552	2871	33	2786	11	2671	24
D0002-2-29	232.50	482.11	0.48	334.46	0.20967	0.00434	14.35776	0.16336	0.49656	0.00532	2903	33	2774	11	2599	23
D0002-2-30	259.45	486.23	0.53	282.79	0.20335	0.00425	11.75290	0.13862	0.41909	0.00455	2853	34	2585	11	2256	21

204

Table 3 LA-ICP MS U-Pb data for zircons from the trondjemitic gneiss (D0002-3) in Northern Kongling terrain.

Grain no.	Pb*(ppm)	Th(ppm)	U(ppm)	Th/U	Isotopic ratio						Age (Ma)					
D0002-3					$^{207}Pb/^{206}Pb$	1σ	$^{207}Pb/^{235}U$	1σ	$^{206}Pb/^{238}U$	1σ	$^{207}Pb/^{206}Pb$	1σ	$^{207}Pb/^{235}U$	1σ	$^{206}Pb/^{238}U$	1σ
D0002-3-1	107.61	147.14	125.01	1.18	0.22156	0.00479	16.39611	0.21174	0.53656	0.00615	2992	34	2900	12	2769	26
D0002-3-2	149.68	180.48	164.34	1.10	0.21542	0.00462	17.20949	0.21831	0.57922	0.00658	2947	34	2947	12	2946	27
D0002-3-3	39.54	30.61	48.42	0.63	0.22414	0.00519	17.06901	0.27051	0.55215	0.00722	3011	37	2939	15	2834	30
D0002-3-4	158.32	116.63	197.87	0.59	0.22426	0.00488	17.19749	0.22794	0.55600	0.00649	3012	35	2946	13	2850	27
D0002-3-5	200.40	65.32	347.35	0.19	0.20488	0.00436	12.34743	0.15100	0.43695	0.00482	2866	34	2631	11	2337	22
D0002-3-6	90.91	68.36	111.42	0.61	0.21259	0.00491	16.95062	0.26774	0.57812	0.00752	2925	37	2932	15	2941	31
D0002-3-7	18.34	11.71	21.64	0.54	0.20915	0.00553	16.96750	0.35967	0.58820	0.00945	2899	42	2933	20	2982	38
D0002-3-8	23.08	19.27	27.57	0.70	0.21254	0.00541	16.81474	0.33040	0.57360	0.00871	2925	41	2924	19	2923	36
D0002-3-9	64.00	53.38	75.84	0.70	0.21437	0.00498	17.04990	0.27361	0.57666	0.00759	2939	37	2938	15	2935	31
D0002-3-10	193.22	92.25	400.24	0.23	0.19449	0.00408	9.64752	0.11159	0.35966	0.00385	2781	34	2402	11	1981	18
D0002-3-11	133.70	77.39	164.95	0.47	0.21654	0.00459	17.32460	0.21086	0.58010	0.00644	2955	34	2953	12	2949	26
D0002-3-12	138.12	248.24	132.74	1.87	0.21570	0.00469	17.20502	0.22897	0.57831	0.00676	2949	35	2946	13	2942	28
D0002-3-13	150.22	104.90	181.83	0.58	0.21505	0.00454	17.15403	0.20571	0.57835	0.00637	2944	34	2944	12	2942	26
D0002-3-14	130.84	193.24	133.47	1.45	0.22100	0.00519	17.92365	0.29706	0.58804	0.00797	2988	37	2986	16	2982	32
D0002-3-15	47.15	44.18	55.08	0.80	0.21313	0.00629	16.91946	0.43424	0.57558	0.01087	2930	47	2930	25	2931	44

Preprints (www.preprints.org) | NOT PEER-REVIEWED | Posted: 8 October 2019 doi:10.20944/preprints201910.0075.v1

D0002-3-16	95.61	38.53	122.29	0.32	0.21380	0.00467	17.00078	0.23031	0.57653	0.00681	2935	35	2935	13	2935	28
D0002-3-17	41.26	25.06	51.19	0.49	0.21313	0.00694	16.84663	0.50167	0.57312	0.01230	2930	52	2926	29	2921	50
D0002-3-18	108.16	102.81	122.34	0.84	0.22268	0.00556	18.12494	0.34588	0.59015	0.00888	3000	40	2996	18	2990	36
D0002-3-19	199.95	87.35	264.36	0.33	0.21197	0.00447	16.74180	0.20083	0.57267	0.00630	2921	34	2920	11	2919	26
D0002-3-20	18.01	14.45	20.50	0.70	0.22389	0.00853	18.29148	0.68037	0.59235	0.01584	3009	60	3005	36	2999	64
D0002-3-21	225.48	79.44	962.35	0.08	0.15038	0.00320	3.96276	0.04775	0.19106	0.00205	2350	36	1627	10	1127	11
D0002-3-22	72.59	65.85	85.34	0.77	0.21040	0.00492	16.90555	0.27718	0.58257	0.00778	2909	37	2930	16	2959	32
D0002-3-23	111.39	77.44	132.84	0.58	0.21523	0.00456	17.19281	0.21008	0.57918	0.00645	2945	34	2946	12	2945	26
D0002-3-24	29.54	27.61	32.98	0.84	0.22047	0.00521	17.90085	0.30206	0.58871	0.00807	2984	38	2984	16	2984	33
D0002-3-25	277.93	140.36	572.87	0.25	0.19976	0.00418	10.41645	0.12048	0.37808	0.00405	2824	34	2473	11	2067	19
D0002-3-26	51.50	51.46	71.06	0.72	0.21874	0.00515	14.58897	0.24030	0.48358	0.00642	2971	37	2789	16	2543	28
D0002-3-27	58.71	51.81	68.58	0.76	0.21437	0.00473	17.06867	0.23956	0.57730	0.00697	2939	35	2939	13	2938	28
D0002-3-28	132.99	68.51	165.71	0.41	0.21470	0.00454	17.10603	0.20837	0.57769	0.00642	2941	34	2941	12	2939	26
D0002-3-29	303.35	630.74	528.76	1.19	0.20239	0.00424	11.23078	0.13153	0.40234	0.00434	2846	34	2543	11	2180	20
D0002-3-30	93.83	120.29	251.92	0.48	0.18497	0.00403	7.01708	0.09166	0.27507	0.00308	2698	36	2114	12	1567	16

Table 4 LA-ICP MS U-Pb data for zircons from the granite dike (D0002-4) in Northern Kongling terrain.

Grain no.					Isotopic ratio						Age (Ma)					
D0002-4	Pb*(ppm)	Th(ppm)	U(ppm)	Th/U	$^{207}Pb/^{207Pb}$	1σ	$^{207}Pb/^{235}U$	1σ	$^{206}Pb/^{238}U$	1σ	$^{207}Pb/^{207Pb}$	1σ	$^{207}Pb/^{235}U$	1σ	$^{206}Pb/^{238}U$	1σ
D0002-4-1	452.64	269.44	586.96	0.46	0.21772	0.00459	16.92001	0.19602	0.56357	0.00610	2964	34	2930	11	2881	25
D0002-4-2	378.07	292.30	468.86	0.62	0.21294	0.00446	16.89237	0.19203	0.57526	0.00617	2928	34	2929	11	2929	25

 doi:10.20944/preprints201910.0075.v1

D0002-4-3	252.13	199.68	1550.91	0.13	0.15489	0.00342	2.82098	0.03719	0.13207	0.00146	2401	37	1361	10	800	8
D0002-4-4	277.35	68.82	505.76	0.14	0.20683	0.00434	12.31505	0.14066	0.43178	0.00463	2881	34	2629	11	2314	21
D0002-4-5	239.31	191.52	294.30	0.65	0.21365	0.00459	16.96291	0.21288	0.57575	0.00651	2933	34	2933	12	2931	27
D0002-4-6	215.10	119.16	276.25	0.43	0.21670	0.00466	17.17466	0.21718	0.57474	0.00654	2956	34	2945	12	2927	27
D0002-4-7	311.49	61.30	437.46	0.14	0.20576	0.00441	15.92407	0.19877	0.56121	0.00632	2872	34	2872	12	2872	26
D0002-4-8	283.46	237.11	518.31	0.46	0.21169	0.00448	11.79217	0.13987	0.40395	0.00442	2919	34	2588	11	2187	20
D0002-4-9	172.37	198.56	1530.00	0.13	0.13223	0.00282	1.57259	0.01900	0.08624	0.00093	2128	37	959	8	533	6
D0002-4-10	377.06	192.79	488.48	0.39	0.21609	0.00465	17.16684	0.21910	0.57607	0.00660	2952	34	2944	12	2933	27
D0002-4-11	356.85	140.21	957.06	0.15	0.18997	0.00397	7.55915	0.08625	0.28854	0.00309	2742	34	2180	10	1634	15
D0002-4-12	409.96	225.81	700.13	0.32	0.20829	0.00433	12.74304	0.14339	0.44363	0.00474	2892	33	2661	11	2367	21
D0002-4-13	283.27	168.77	372.12	0.45	0.20674	0.00463	16.05492	0.23392	0.56312	0.00696	2880	36	2880	14	2880	29
D0002-4-14	287.63	142.04	476.37	0.30	0.20161	0.00433	13.18388	0.16751	0.47418	0.00538	2839	35	2693	12	2502	24
D0002-4-15	229.15	199.70	1384.15	0.14	0.15340	0.00324	2.69507	0.03200	0.12739	0.00137	2384	36	1327	9	773	8
D0002-4-16	286.64	162.70	368.78	0.44	0.21473	0.00448	17.10041	0.19814	0.57748	0.00630	2942	33	2941	11	2939	26
D0002-4-17	164.60	73.23	214.07	0.34	0.21378	0.00488	16.98473	0.26240	0.57611	0.00744	2934	36	2934	15	2933	30
D0002-4-18	289.34	92.12	384.40	0.24	0.21399	0.00445	17.01132	0.19709	0.57646	0.00629	2936	33	2936	11	2934	26
D0002-4-19	507.49	549.26	588.41	0.93	0.21659	0.00451	17.20146	0.19979	0.57589	0.00630	2956	33	2946	11	2932	26
D0002-4-20	500.19	312.08	633.03	0.49	0.20720	0.00428	16.08722	0.18214	0.56301	0.00607	2884	33	2882	11	2879	25
D0002-4-21	446.49	272.93	669.57	0.41	0.21259	0.00438	14.46536	0.16228	0.49342	0.00530	2925	33	2781	11	2585	23
D0002-4-22	201.28	78.91	264.04	0.30	0.21624	0.00448	17.20104	0.19863	0.57682	0.00630	2953	33	2946	11	2936	26

D0002-4-23	399.31	201.86	509.82	0.40	0.21389	0.00444	17.01827	0.19758	0.57697	0.00632	2935	33	2936	11	2936	26
D0002-4-24	430.69	394.84	969.34	0.41	0.19797	0.00410	9.16837	0.10519	0.33583	0.00363	2810	33	2355	11	1867	18
D0002-4-25	353.71	183.19	465.75	0.39	0.20767	0.00436	16.20711	0.19865	0.56594	0.00638	2887	34	2889	12	2891	26
D0002-4-26	360.46	118.91	624.71	0.19	0.19502	0.00401	11.98605	0.13577	0.44569	0.00481	2785	33	2603	11	2376	21
D0002-4-27	235.28	101.81	387.86	0.26	0.19727	0.00427	12.61007	0.16851	0.46354	0.00542	2804	35	2651	13	2455	24
D0002-4-28	403.55	180.05	905.10	0.20	0.18702	0.00385	9.01205	0.10275	0.34943	0.00378	2716	34	2339	10	1932	18
D0002-4-29	285.80	36.32	433.39	0.08	0.20221	0.00416	14.71022	0.16840	0.52753	0.00574	2844	33	2797	11	2731	24
D0002-4-30	480.98	1336.66	743.74	1.80	0.19759	0.00404	12.82957	0.14272	0.47084	0.00505	2806	33	2667	10	2487	22
D0002-4-31	279.86	60.53	385.19	0.16	0.20755	0.00431	16.14779	0.19164	0.56419	0.00627	2887	33	2886	11	2884	26
D0002-4-32	461.35	495.88	794.85	0.62	0.20797	0.00426	12.08947	0.13679	0.42155	0.00456	2890	33	2611	11	2268	21
D0002-4-33	454.78	299.99	665.25	0.45	0.21142	0.00432	14.72818	0.16505	0.50520	0.00545	2916	33	2798	11	2636	23
D0002-4-34	133.25	124.22	153.68	0.81	0.21896	0.00497	17.67433	0.27795	0.58537	0.00773	2973	36	2972	15	2971	31
D0002-4-35	604.82	208.02	1032.70	0.20	0.19563	0.00403	12.35619	0.14363	0.45805	0.00502	2790	33	2632	11	2431	22
D0002-4-36	377.29	69.06	611.44	0.11	0.19858	0.00404	13.40386	0.14965	0.48950	0.00528	2815	33	2709	11	2569	23

206

207 **Table 5** LA-ICP MS U-Pb data for zircons from the moyite dike (D0002-5) in Northern Kongling terrain.

Grain no.	Pb*(ppm)	Th(ppm)	U(ppm)	Th/U	Isotopic ratio						Age (Ma)					
D0002-5					$^{207}Pb/^{207Pb}$	1σ	$^{207}Pb/^{235}U$	1σ	$^{206}Pb/^{238}U$	1σ	$^{207}Pb/^{207Pb}$	1σ	$^{207}Pb/^{235}U$	1σ	$^{206}Pb/^{238}U$	1σ
D0002-5-1	307.71	42.70	596.95	0.07	0.20063	0.00415	11.31110	0.13013	0.40882	0.00444	2831	33	2549	11	2210	20
D0002-5-2	176.79	30.18	269.84	0.11	0.20340	0.00423	14.46363	0.17181	0.51563	0.00570	2854	34	2781	11	2681	24
D0002-5-3	242.04	89.79	551.50	0.16	0.19427	0.00409	9.05285	0.11038	0.33791	0.00375	2779	34	2343	11	1877	18
D0002-5-4	364.18	36.97	773.38	0.05	0.19627	0.00403	10.22766	0.11497	0.37787	0.00406	2795	33	2456	10	2066	19

D0002-5-5	327.09	102.62	435.82	0.24	0.21040	0.00436	16.51837	0.19383	0.56931	0.00627	2909	33	2907	11	2905	26
D0002-5-6	284.40	87.65	388.07	0.23	0.20629	0.00431	15.99756	0.19323	0.56232	0.00628	2877	34	2877	12	2876	26
D0002-5-7	353.44	67.18	855.57	0.08	0.20111	0.00414	9.03830	0.10254	0.32589	0.00351	2835	33	2342	10	1819	17
D0002-5-8	219.47	46.91	381.02	0.12	0.20180	0.00419	12.51861	0.14697	0.44983	0.00493	2841	33	2644	11	2395	22
D0002-5-9	105.86	70.16	136.47	0.51	0.20403	0.00430	15.68575	0.19438	0.55749	0.00631	2859	34	2858	12	2856	26
D0002-5-10	290.26	67.75	456.12	0.15	0.20386	0.00419	13.87859	0.15654	0.49366	0.00532	2857	33	2742	11	2587	23
D0002-5-11	299.39	69.41	454.87	0.15	0.20828	0.00428	14.79864	0.16822	0.51521	0.00558	2892	33	2802	11	2679	24
D0002-5-12	258.99	38.76	363.26	0.11	0.20765	0.00437	16.14538	0.19925	0.56382	0.00637	2887	34	2885	12	2882	26
D0002-5-13	329.34	53.01	587.40	0.09	0.20254	0.00421	12.43787	0.14718	0.44530	0.00490	2847	34	2638	11	2374	22
D0002-5-14	314.96	28.65	515.92	0.06	0.20980	0.00438	14.03975	0.16881	0.48526	0.00540	2904	33	2752	11	2550	23
D0002-5-15	369.54	38.67	516.14	0.07	0.21184	0.00444	16.64215	0.20378	0.56965	0.00642	2920	34	2914	12	2906	26
D0002-5-16	321.50	120.49	696.50	0.17	0.19873	0.00408	10.02235	0.11314	0.36569	0.00394	2816	33	2437	10	2009	19
D0002-5-17	369.05	43.47	676.32	0.06	0.20105	0.00416	12.18874	0.14111	0.43961	0.00479	2835	33	2619	11	2349	21
D0002-5-18	306.54	80.08	626.93	0.13	0.19954	0.00413	10.81604	0.12570	0.39306	0.00428	2822	33	2507	11	2137	20
D0002-5-19	304.80	35.32	433.02	0.08	0.20658	0.00426	16.01814	0.18457	0.56227	0.00613	2879	33	2878	11	2876	25
D0002-5-20	402.30	34.15	565.47	0.06	0.21002	0.00431	16.51470	0.18715	0.57021	0.00617	2906	33	2907	11	2909	25
D0002-5-21	394.93	361.68	######	0.27	0.19387	0.00406	5.62481	0.06718	0.21038	0.00230	2775	34	1920	10	1231	12
D0002-5-22	171.47	20.47	241.75	0.08	0.20519	0.00429	15.98548	0.19359	0.56491	0.00631	2868	34	2876	12	2887	26
D0002-5-23	243.93	48.12	394.78	0.12	0.21002	0.00435	14.11409	0.16520	0.48731	0.00534	2906	33	2757	11	2559	23
D0002-5-24	328.84	52.83	630.54	0.08	0.20634	0.00426	11.83753	0.13660	0.41600	0.00452	2877	33	2592	11	2242	21

208

Preprints (www.preprints.org) | NOT PEER-REVIEWED | Posted: 8 October 2019 doi:10.20944/preprints201910.0075.v1

209 **Table 6 Re**presentative major (wt. %) and trace element (ppm) concentrations of the Biotite
210 tremolite-schist, Archean TTG and dikes in Northern Kongling terrain.

Sample	D0002-1	D0002-2	SMK-4	D0002-3	SMK-1	D0002-4	D0002-5
	Bi-Ttremolite-schist	Tonalitic gneiss		Trondhjemite gneiss		Granite dike	
SiO_2	54.71	76.80	70.86	76.08	69.79	73.92	78.74
TiO_2	0.24	0.09	0.29	0.16	0.43	0.18	0.03
Al_2O_3	2.78	13.77	15.82	14.08	15.49	13.11	12.85
FeO_{total}	6.65	0.55	2.05	0.57	2.19	1.12	0.24
MnO	0.24	0.01	0.03	0.01	0.03	0.02	0.01
MgO	20.81	0.29	0.81	0.30	1.02	0.28	0.16
CaO	10.28	0.91	2.82	0.75	2.48	1.21	0.85
Na_2O	0.11	5.98	4.98	6.67	4.55	4.41	5.98
K_2O	1.46	0.88	1.53	0.70	2.62	4.28	0.52
P_2O_5	0.01	0.02	0.06	0.05	0.12	0.08	0.02
LOI	1.53	0.49	0.37	0.47	0.71	0.98	0.47
Total	98.82	99.78	99.62	99.84	99.43	99.59	99.87
Mg#	85.00	47.00	41.00	47.00	45.00	30.00	55.00
K_2O+Na_2O	1.57	6.86	6.51	7.37	7.17	8.69	6.50
K_2O/Na_2O	12.80	0.15	0.31	0.11	0.58	0.97	0.09
A/CNK	0.14	1.11	1.06	1.07	1.05	0.93	1.08
V	56.4	7.68	19.66	8.38	43.64	18.4	4.1
Cr	1800	3.39	9.48	1.7	12.32	6.66	1.52
Co	106	1.52	55.49	1.33	61.78	2.13	＜1
Ni	1630	2.87	7.17	3.14	8.41	4.88	3.29
Ga	7.5	33.6	15.24	20.8	53.29	63.6	24.5
Rb	94.7	23.4	75.44	26.3	56.78	76.5	16.5
Sr	20.5	311	370.39	196	437.36	243	342
Y	5.9	7.89	6.27	4.82	9.28	10.6	12.2
Zr	29.8	66.1	102.94	91.6	248.84	215	61.7
Nb	1.26	3.1	6.66	3.01	6.1	2.8	2.74
Ba	121	947	186.83	312	159.08	2540	306
La	1.19	28.6	18.5	14.8	24.32	148	15.8
Ce	3.05	39.7	29.38	19.6	39.93	195	20.4
Pr	0.62	5.53	3.33	2.76	5.05	18.1	2.98
Nd	3.07	20	11.18	10	18.31	60.4	11.6
Sm	0.88	3.47	1.65	1.76	3.12	8.37	2.55
Eu	0.24	1.05	0.74	0.8	1.49	1.69	0.7
Gd	0.86	2.79	1.42	1.55	2.74	6.67	2.29
Tb	0.16	0.34	0.2	0.22	0.35	0.66	0.38
Dy	1.1	1.6	1.13	1.08	1.81	2.46	2.28
Ho	0.24	0.29	0.23	0.19	0.34	0.41	0.46
Er	0.64	0.76	0.73	0.46	0.97	1.04	1.24
Tm	0.1	0.11	0.12	0.062	0.14	0.11	0.2
Yb	0.71	0.74	0.87	0.36	0.92	0.68	1.29
Lu	0.1	0.1	0.14	0.044	0.14	0.086	0.18
Hf	0.98	2.99	3.21	2.88	6.29	5.29	4.45
Ta	0.099	0.41	0.56	0.088	0.54	0.097	0.43
Pb	3.38	8.71	19.4	5.88	19.27	12.4	10.8
Th	0.19	12.5	4.95	1.63	7.26	11.5	13.6
U	0.42	1.6	0.41	0.36	1	0.49	5.49
La_N/Yb_N	1.2	27.72	15.3	29.49	18.88	156.12	8.79
Eu/Eu*	0.83	1	1.42	1.45	1.52	0.67	0.87
1000 Ga/Al	5.4	4.88	0.36	2.95	0.32	9.7	3.81
Total REE	12.96	105.08	69.62	53.69	99.65	443.68	62.35

211

212 **Table 7 Lu-Hf isotope data for zircons from the Biotite tremolite-schist, Archean TTG and dikes in Nor**thern Kongling terrain.

Sample	$^{176}Hf/^{177}Hf$	1σ	$^{176}Lu/^{177}Hf$	1σ	$^{176}Yb/^{177}Hf$	1σ	Age (Ma)	$^{176}Hf/^{177}Hf$ (t)	$\varepsilon_{Hf}(t)$	1σ	T_{DM1}	T_{DM2}	$f_{Lu/Hf}$
D0002-1-01	0.280951	0.000022	0.000407	0.000002	0.008177	0.000031	2953	0.280927	1.3	1.1	3.15	3.23	-0.99
D0002-1-02	0.280855	0.000014	0.000404	0.000003	0.008611	0.000039	2941	0.280833	-2.4	0.9	3.27	3.41	-0.99
D0002-1-03	0.280835	0.000012	0.000486	0.000004	0.010876	0.000113	2932	0.280808	-3.5	0.8	3.31	3.46	-0.99
D0002-1-04	0.280890	0.000018	0.000327	0.000002	0.006678	0.000024	2912	0.280872	-1.7	1.0	3.22	3.35	-0.99
D0002-1-05	0.280916	0.000024	0.000474	0.000003	0.010331	0.000080	2930	0.280890	-0.6	1.1	3.20	3.31	-0.99
D0002-1-06	0.280917	0.000018	0.000384	0.000005	0.008261	0.000050	2955	0.280895	0.1	1.0	3.19	3.29	-0.99
D0002-1-07	0.280838	0.000010	0.000536	0.000003	0.012015	0.000112	2846	0.280809	-5.5	0.8	3.31	3.50	-0.98
D0002-1-08	0.280786	0.000012	0.000260	0.000004	0.005863	0.000093	2918	0.280771	-5.1	0.8	3.35	3.54	-0.99
D0002-1-09	0.280869	0.000011	0.001473	0.000064	0.048796	0.002518	3034	0.280784	-2.0	0.9	3.35	3.46	-0.96
D0002-1-10	0.280926	0.000018	0.000423	0.000006	0.010519	0.000087	3001	0.280902	1.5	1.0	3.18	3.26	-0.99
D0002-1-11	0.280961	0.000015	0.000399	0.000004	0.009691	0.000113	2957	0.280939	1.7	0.9	3.13	3.21	-0.99
D0002-1-12	0.280875	0.000012	0.000721	0.000002	0.017945	0.000048	2901	0.280834	-3.3	0.8	3.27	3.43	-0.98
D0002-1-13	0.280877	0.000012	0.000847	0.000006	0.020028	0.000231	2913	0.280830	-3.2	0.8	3.28	3.43	-0.97
D0002-1-14	0.280822	0.000016	0.000556	0.000003	0.013783	0.000090	2947	0.280790	-3.8	0.9	3.33	3.49	-0.98
D0002-1-15	0.280831	0.000012	0.000460	0.000003	0.010361	0.000129	2967	0.280804	-2.8	0.8	3.31	3.45	-0.99
D0002-1-16	0.280883	0.000013	0.001490	0.000040	0.052002	0.001677	3021	0.280797	-1.8	0.9	3.33	3.44	-0.96
D0002-2-01	0.280847	0.000010	0.000733	0.000002	0.022362	0.000070	2934	0.280806	-3.5	0.8	3.31	3.47	-0.98
D0002-2-02	0.280872	0.000013	0.001010	0.000010	0.029241	0.000148	2945	0.280815	-3.0	0.9	3.30	3.44	-0.97
D0002-2-03	0.280859	0.000015	0.001520	0.000031	0.045511	0.000942	2956	0.280772	-4.2	0.9	3.36	3.52	-0.95
D0002-2-04	0.280853	0.000012	0.001015	0.000017	0.030518	0.000620	2958	0.280796	-3.3	0.9	3.33	3.47	-0.97
D0002-2-05	0.280844	0.000011	0.000784	0.000036	0.022883	0.001178	2951	0.280800	-3.3	0.9	3.32	3.47	-0.98
D0002-2-06	0.280870	0.000014	0.001882	0.000044	0.057025	0.001497	2948	0.280763	-4.7	0.9	3.38	3.54	-0.94
D0002-2-07	0.280841	0.000015	0.001046	0.000017	0.030454	0.000321	2952	0.280782	-4.0	0.9	3.35	3.50	-0.97
D0002-2-08	0.280868	0.000012	0.001518	0.000031	0.046408	0.001013	2941	0.280783	-4.2	0.9	3.35	3.51	-0.95
D0002-3-01	0.280909	0.000015	0.001418	0.000024	0.043538	0.000698	2992	0.280828	-1.4	0.9	3.29	3.40	-0.96
D0002-3-02	0.280843	0.000013	0.001184	0.000014	0.034520	0.000424	2925	0.280776	-4.8	0.9	3.36	3.52	-0.96
D0002-3-05	0.280889	0.000015	0.001882	0.000014	0.058348	0.000387	2988	0.280781	-3.2	0.9	3.36	3.49	-0.94

D0002-3-06	0.280793	0.000009	0.000684	0.000016	0.020283	0.000417	3009	0.280754	-3.6	0.8	3.38	3.53	-0.98
D0002-3-07	0.280870	0.000013	0.001423	0.000015	0.042550	0.000518	2945	0.280790	-3.8	0.9	3.34	3.49	-0.96
D0002-3-08	0.280844	0.000013	0.000642	0.000012	0.019083	0.000451	2984	0.280807	-2.3	0.9	3.31	3.44	-0.98
D0002-3-09	0.280867	0.000015	0.001473	0.000006	0.043742	0.000368	2939	0.280784	-4.2	0.9	3.35	3.50	-0.96
D0002-4-01	0.280900	0.000013	0.001646	0.000045	0.050871	0.001707	2964	0.280807	-2.8	0.9	3.32	3.45	-0.95
D0002-4-02	0.280856	0.000011	0.000579	0.000006	0.017595	0.000264	2872	0.280824	-4.3	0.8	3.29	3.46	-0.98
D0002-4-03	0.280913	0.000016	0.001225	0.000019	0.040155	0.000434	2933	0.280844	-2.2	0.9	3.27	3.39	-0.96
D0002-4-04	0.280813	0.000012	0.001099	0.000020	0.029884	0.000733	2952	0.280751	-5.1	0.9	3.39	3.56	-0.97
D0002-4-05	0.280910	0.000011	0.001667	0.000033	0.049941	0.001195	2880	0.280818	-4.3	0.8	3.31	3.47	-0.95
D0002-4-06	0.280897	0.000012	0.001006	0.000013	0.031209	0.000358	2942	0.280840	-2.1	0.9	3.27	3.40	-0.97
D0002-4-07	0.280880	0.000011	0.000942	0.000004	0.028800	0.000249	2934	0.280827	-2.8	0.8	3.29	3.43	-0.97
D0002-4-08	0.280874	0.000012	0.001062	0.000011	0.032768	0.000244	2936	0.280814	-3.2	0.8	3.30	3.45	-0.97
D0002-4-09	0.280830	0.000015	0.001237	0.000021	0.037397	0.000921	2956	0.280760	-4.6	0.9	3.38	3.54	-0.96
D0002-4-10	0.280907	0.000011	0.001973	0.000013	0.065697	0.000407	2884	0.280798	-4.9	0.8	3.34	3.50	-0.94
D0002-4-11	0.280879	0.000012	0.001324	0.000009	0.041879	0.000096	2953	0.280804	-3.1	0.9	3.32	3.46	-0.96
D0002-4-12	0.280941	0.000012	0.002114	0.000107	0.070993	0.004036	2935	0.280822	-2.9	1.0	3.30	3.43	-0.94
D0002-4-13	0.280908	0.000012	0.001696	0.000029	0.051172	0.001052	2887	0.280814	-4.3	0.9	3.31	3.47	-0.95
D0002-4-14	0.280879	0.000009	0.001193	0.000021	0.034871	0.000890	2887	0.280813	-4.4	0.8	3.31	3.47	-0.96
D0002-5-01	0.280920	0.000020	0.001397	0.000015	0.038193	0.000434	2909	0.280842	-2.8	1.0	3.27	3.41	-0.96
D0002-5-02	0.280888	0.000010	0.001054	0.000016	0.030283	0.000378	2877	0.280830	-4.0	0.8	3.28	3.44	-0.97
D0002-5-03	0.280845	0.000013	0.000937	0.000020	0.028552	0.000584	2859	0.280793	-5.7	0.9	3.33	3.52	-0.97
D0002-5-04	0.280900	0.000024	0.001250	0.000008	0.034076	0.000142	2887	0.280830	-3.7	1.1	3.29	3.44	-0.96
D0002-5-05	0.280909	0.000018	0.001086	0.000031	0.030378	0.000766	2920	0.280848	-2.3	1.0	3.26	3.39	-0.97
D0002-5-06	0.280859	0.000009	0.001239	0.000027	0.039478	0.000984	2879	0.280790	-5.4	0.8	3.34	3.52	-0.96
D0002-5-07	0.280880	0.000012	0.001151	0.000012	0.032658	0.000295	2906	0.280816	-3.8	0.8	3.30	3.46	-0.97
D0002-5-08	0.280869	0.000017	0.000540	0.000007	0.015970	0.000183	2868	0.280839	-3.9	0.9	3.27	3.43	-0.98

213 Note: a, Initial Hf isotope ratios are calculated nearly by their Age of single grain zircon; b, T_{DM2} are calculated by assuming a mean $^{176}Lu/^{177}Hf$ value of 0.015 for the average continental crust[30].

214

Preprints (www.preprints.org) | NOT PEER-REVIEWED | Posted: 8 October 2019 doi:10.20944/preprints201910.0075.v1

4.1.2. TTG Gneiss

The zircon grains from the tonalitic gneiss (D0002-2) have different features from the zircons of the biotite–tremolite schist sample D0002-1, described above. Thirty spots on 25 grains were analyzed (Table 2), and most of the U–Pb isotopic data are discordant (Figure 7). All analyzed spots gave an upper intercept age of 2943 ± 15 Ma (MSWD = 8.4, n = 25), and eight of the grains form a tight population with a weighted mean $^{207}Pb/^{206}Pb$ age of 2948 ± 26 Ma (MSWD = 0.053, n = 8) and a concordant age of 2947 ± 5.6 Ma (MSWD = 0.006), which is within error of the U–Pb age of 2944 ± 22 Ma for zircons from the biotite–tremolite schist (sample D0002-1).

Figure 6. Representative cathodoluminescence images of zircons from the tonalitic gneiss (D0002-2). Symbols are as in Figure 4.

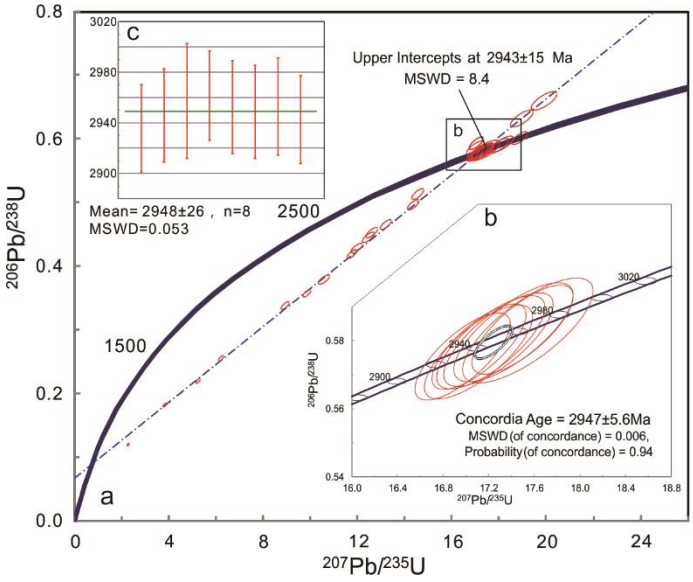

Figure 7. Zircon U–Pb concordia age diagram for the tonalitic gneiss (D0002-2). (a) Diagram for all analytical spots that gave a discordia line with an upper intercept $^{207}Pb/^{206}Pb$ age of 2943 ± 15 Ma. (b) and (c) Diagrams for eight analytical spots that gave a concordant $^{207}Pb/^{206}Pb$ age of 2947 ± 5.6 Ma and a weighted mean $^{207}Pb/^{206}Pb$ age of 2948 ± 26 Ma.

Preprints (www.preprints.org) | NOT PEER-REVIEWED | Posted: 8 October 2019 doi:10.20944/preprints201910.0075.v1

Zircon grains from the trondhjemitic gneiss (D0002-3) are euhedral to subhedral, slightly rounded in form, and display oscillatory zoning in CL images, typical of magmatic zircons (Figure 8). Most of the zircon grains display core–rim structures. The rims are usually very narrow, dark, and structureless, suggesting recrystallization during a later hydrothermal alteration. These rims were too narrow to be analyzed. Thirty spots on 22 grains were analyzed (Table 3), and most of the U–Pb isotopic data are discordant (Figure 9a), suggesting Pb loss caused by a later hydrothermal event. A discordia line of 14 discordant analyses yielded an upper intercept $^{207}Pb/^{206}Pb$ age of 3007 ± 18 Ma (2σ, MSWD = 3, n = 14). The remaining 16 spots with ages of 2955–2899 Ma are nearly concordant (concordance >98%), and they gave a concordant age of $^{207}Pb/^{206}Pb$ age of 2939 ± 4 Ma (2σ, MSWD = 0.18, n = 16; Figure 9b) and a weighted mean $^{207}Pb/^{206}Pb$ age of 2935 ± 9 Ma (2σ, MSWD = 0.6, n = 16; Figure 9c).

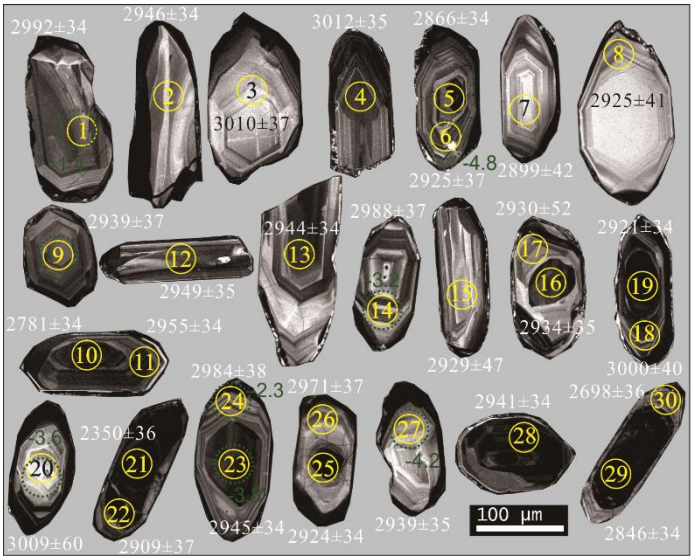

Figure 8. Representative cathodoluminescence images of zircons from the trondhjemitic gneiss (D0002-3). Symbols are as in Figure 4.

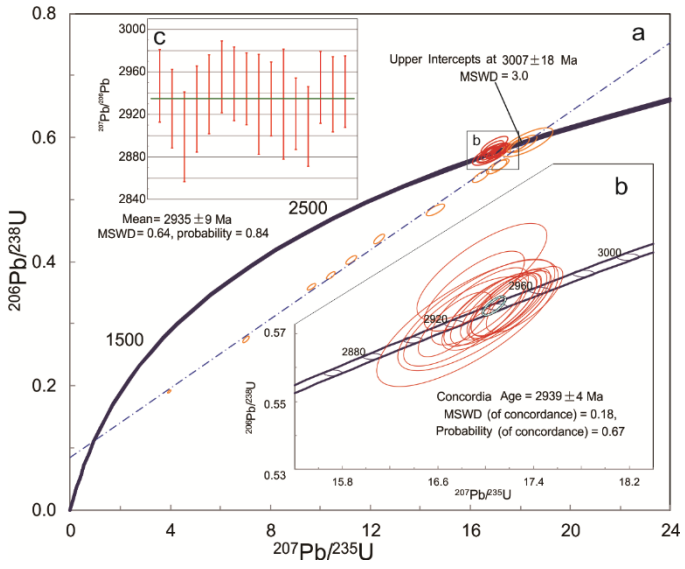

Figure 9. Zircon U–Pb concordia age diagrams for the trondhjemitic gneiss (D0002-3). (a) Diagram for 14 analytical spots that gave a discordia line with an upper intercept $^{207}Pb/^{206}Pb$ age of 3007 ± 18 Ma. (b) and (c) Diagrams for 16 analytical spots that gave a concordant $^{207}Pb/^{206}Pb$ age of 2939 ± 4 Ma and a weighted mean $^{207}Pb/^{206}Pb$ age of 2935 ± 9 Ma.

Preprints (www.preprints.org) | NOT PEER-REVIEWED | Posted: 8 October 2019 doi:10.20944/preprints201910.0075.v1

252 4.1.3. Granite Dikes

253 The zircon grains from the dikes of gneissic granite (D0002-4) are subhedral to anhedral
254 (Figure 10). Most of the zircons display core–rim structures, and they can be divided into two
255 groups by the internal textures of the cores. In group a, the cores have a complicated internal
256 texture with sector zoning but no oscillatory zoning, suggesting a metamorphic origin. In
257 contrast, the zircons of group b display weak sector zoning and obvious oscillatory zoning that
258 is typical of magmatic zircons.

259 Thirty-six spots were analyzed (Table 4), and two discordia lines are present in the zircon
260 U–Pb concordia age diagrams for sample D00002-4. The one discordia line with 18 discordant
261 analyses yielded an upper intercept $^{207}Pb/^{206}Pb$ age of 2881 ± 15 Ma (2σ, MSWD = 0.50, n = 16;
262 Figure 11a), and five analyses gave a concordant age of $^{207}Pb/^{206}Pb$ age of 2882 ± 15 Ma (2σ,
263 MSWD = 0.13, n = 5; Figure 11b). The other discordia line with 18 analyses defined an older
264 upper intercept $^{207}Pb/^{206}Pb$ age of 2944 ± 9 Ma (2σ, MSWD = 0.5, n = 18) and a weighted mean
265 $^{207}Pb/^{206}Pb$ age of 2943 ± 10 Ma (2σ, MSWD = 0.39, n = 10; Figure 11c).

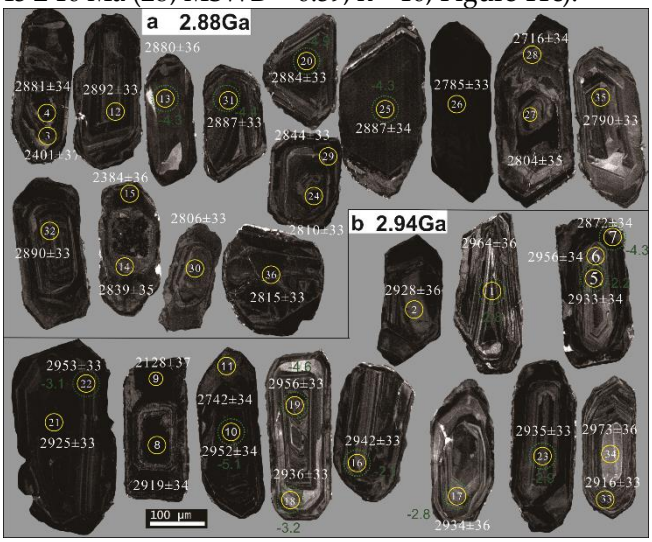

266

267 **Figure 10.** Representative cathodoluminescence images of zircons from the granite dike
268 (D0002-4). Symbols are as in Figure 4.

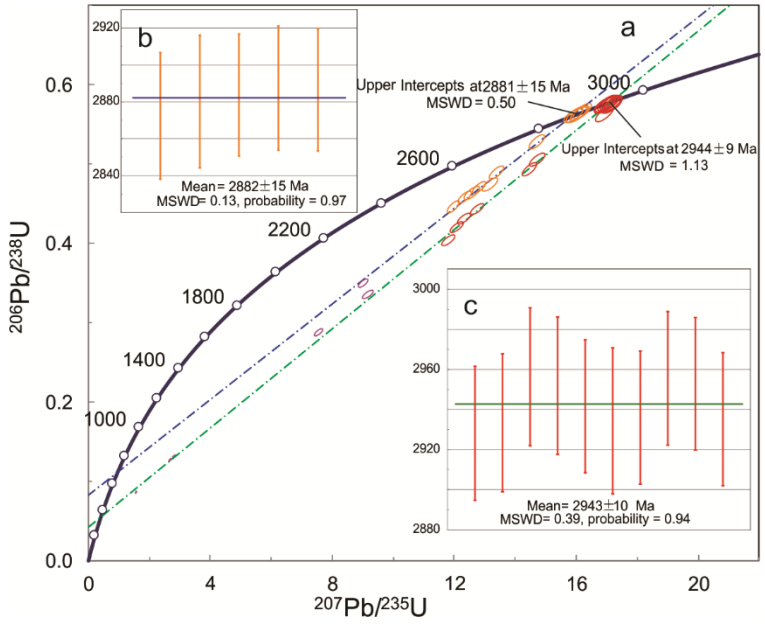

269

Preprints (www.preprints.org) | NOT PEER-REVIEWED | Posted: 8 October 2019 doi:10.20944/preprints201910.0075.v1

Figure 11. Zircon U–Pb concordia age diagrams for the granite dike (D0002-4). (a) Diagram for all analyzed spots that gave two discordia lines with upper intercept $^{207}Pb/^{206}Pb$ ages of 2994 ± 9 Ma and 2881 ± 15 Ma. (b) Diagram for five concordant analyses that gave a weighted mean $^{207}Pb/^{206}Pb$ age of 2882 ± 15 Ma. (c) Diagram for 10 concordant analyses that gave a weighted mean $^{207}Pb/^{206}Pb$ age of 2943 ± 10 Ma.

The zircon grains from the moyite dike (D0002-5) (Figure 12) are smaller but otherwise similar to those from granite dike D0002-4. Twenty-four spots on 22 grains were analyzed (Table 5), and most of the U–Pb isotopic data were discordant (Figure 13a), suggesting Pb loss caused by a later hydrothermal event. A discordia line with 16 discordant analyses yielded an upper intercept $^{207}Pb/^{206}Pb$ age of 2874 ± 11 Ma (2σ, MSWD = 0.43, n = 16), and another 5 analyses gave a concordant $^{207}Pb/^{206}Pb$ age of 2874 ± 15 Ma (2σ, MSWD = 0.42, n = 3; Figure 13b). The remaining eight spots defined an older upper intercept $^{207}Pb/^{206}Pb$ age of 2910 ± 11 Ma (2σ, MSWD = 0.49, n = 8) and a weighted mean $^{207}Pb/^{206}Pb$ age of 2911 ± 19 Ma (2σ, MSWD = 0.20, n = 3; Figure 13c).

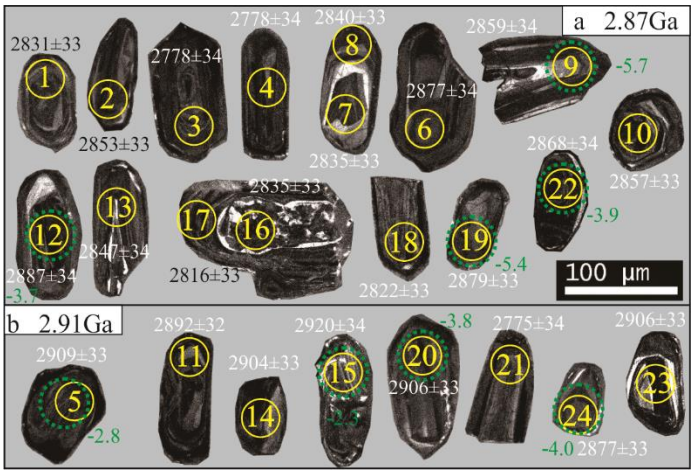

Figure 12. Representative cathodoluminescence images of zircons from the moyite dike (D0002-5). Symbols are as in Figure 4.

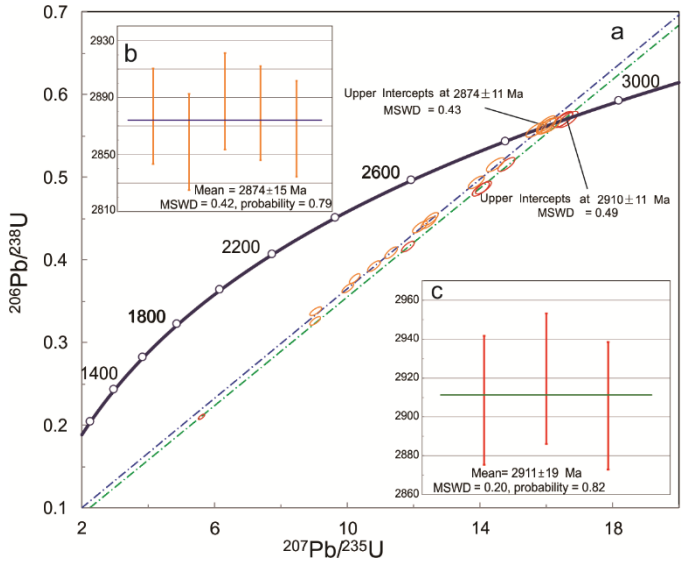

Figure 13. Zircon U–Pb concordia age diagrams for the moyite dike (D0002-5). (a) Diagram for all analyzed spots that gave two discordia lines with two upper intercept $^{207}Pb/^{206}Pb$ ages of 2910 ± 11 Ma and 2874 ± 11 Ma. (b) Diagram for five concordant analyses that gave a weighted mean $^{207}Pb/^{206}Pb$ age of 2874 ± 15 Ma. (c) Diagram for three concordant analyses that gave a weighted mean $^{207}Pb/^{206}Pb$ age of 2911 ± 19 Ma.

Preprints (www.preprints.org) | NOT PEER-REVIEWED | Posted: 8 October 2019 doi:10.20944/preprints201910.0075.v1

293 *4.2. Whole-rock major and trace element compositions*

294 4.2.1. Biotite Tremolite-schist

295 The results of the major and trace element analyses of the five samples are presented in
296 Table 6. The samples from the Yemadong Group display relatively low contents of SiO_2 (30.24–
297 54.71 wt%, average 46.23 wt%) and Al_2O_3 (2.78–6.36 wt%, average 5.01 wt%), but relatively high
298 contents of MgO (19.27–27.01 wt%, average 22.88 wt%). The samples can be divided into two
299 series by their total alkali contents ($Na_2O + K_2O$). The three samples of the first series (D050-1,
300 D050-2, and D0002-1) have relatively high total alkali contents (1.57–3.69 wt%, average 2.86
301 wt%), and the other two samples display lower contents (0.29 wt% and 0.41 wt%).

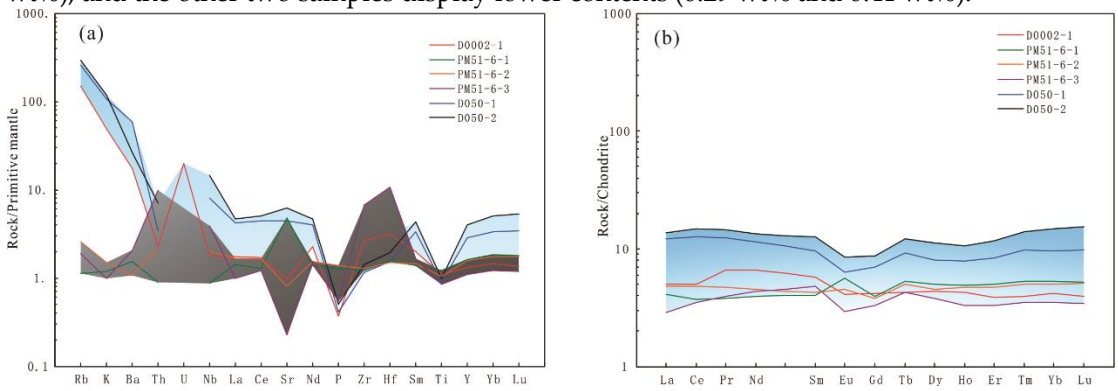

302

303 **Figure 14.** (a) Primitive-mantle-normalized trace element distributions and (b) chondrite-
304 normalized rare earth element patterns for the biotite–tremolite schist enclaves from the
305 Kongling Terrane. Normalizing values are from McDonough and Sun (1989).

306 The trace element compositions of the first series of samples (D050-1, D050-2, and D0002-
307 1) show strong enrichments in large ion lithophile elements (LILEs; e.g., K, Rb, Ba, and Th) and
308 depletions in high field strength elements (HFSEs; e.g., Nb, Ta, P, and Ti; Figure 14a). The other
309 two samples show depletions in LILEs and enrichments in HFSEs. All five samples have very
310 high Cr (>1300 ppm) and Ni (>800 ppm) contents.

311 In summary, the biotite–tremolite schists possess lower total REE values (9.46–33.12 ppm),
312 relatively flat REE patterns (average $(La/Yb)_N$ ratio of 0.99; Figure 14b), and both positive and
313 negative Eu anomalies (δEu = 0.73–1.40). The protoliths of the biotite–tremolite schists were
314 basic–intermediate magmatic rocks of the calc-alkaline series, including rhyodacite, dacite,
315 basalt, or basaltic andesite (Figure 15). On a TAS volcanic rock classification diagram, all the
316 Archean metabasite samples fall into the basaltic andesite and calc-alkaline series fields.

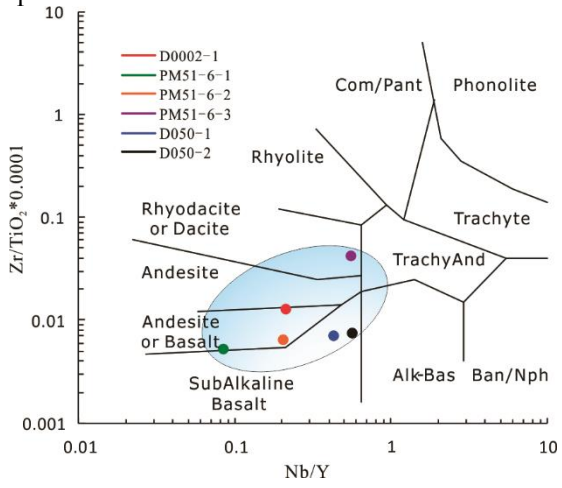

317

Preprints (www.preprints.org) | NOT PEER-REVIEWED | Posted: 8 October 2019 doi:10.20944/preprints201910.0075.v1

Figure 15. Classification of the biotite–tremolite schist enclaves from the Kongling Terrane using the Nb/Y vs Zr/Ti diagram after Winchester and Floyd (1977) and modified by Pearce (1996).

4.2.2. TTG Gneiss

The major and trace element compositions of the TGG gneissic rocks are listed in Table 6. According to their normative feldspar compositions, two samples are recognized as trondhjemites, sample SMK-1 falls near the granodiorite field, and sample SMK-4 falls close to the tonalite field (Figure 16a). All the samples display relatively high contents of SiO_2 (69.79–76.80 wt%, Figure 16b), Al_2O_3 (13.77–15.82 wt%, Figure 17), and total alkalis ($Na_2O + K_2O$; 6.51–7.37 wt%), high values of $Mg^{\#}$ (41–47), and comparatively low contents of K_2O (0.70–2.62 wt%, Figure 17), TiO_2 (0.09–0.43 wt%, Figure 17), FeO^T (0.55–2.19 wt%, Figure17), and MgO (0.29–1.02 wt%) (Figure 16b). They are magnesian and weakly peraluminous (A/CNK 1.05–1.11) (Figure 16c).

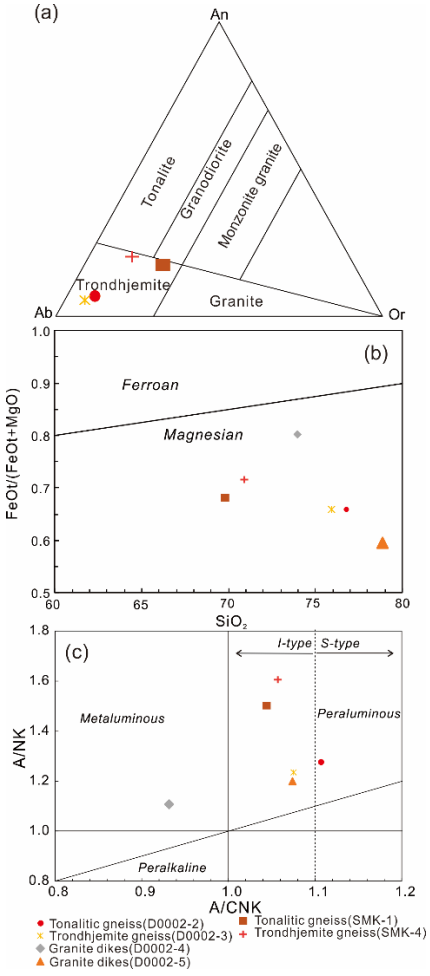

Figure 16. (a): The TTG suite of rocks plotted on the CIPW an–ab–or classification diagram (after [31]). An = anorthite, Ab = albite, Or = orthoclase; $FeO^t/(FeO^t+MgO)$-SiO_2 classification diagram (after [32]);A/NK-A/CNK diagram of granitoids (after [33]).

Preprints (www.preprints.org) | NOT PEER-REVIEWED | Posted: 8 October 2019 doi:10.20944/preprints201910.0075.v1

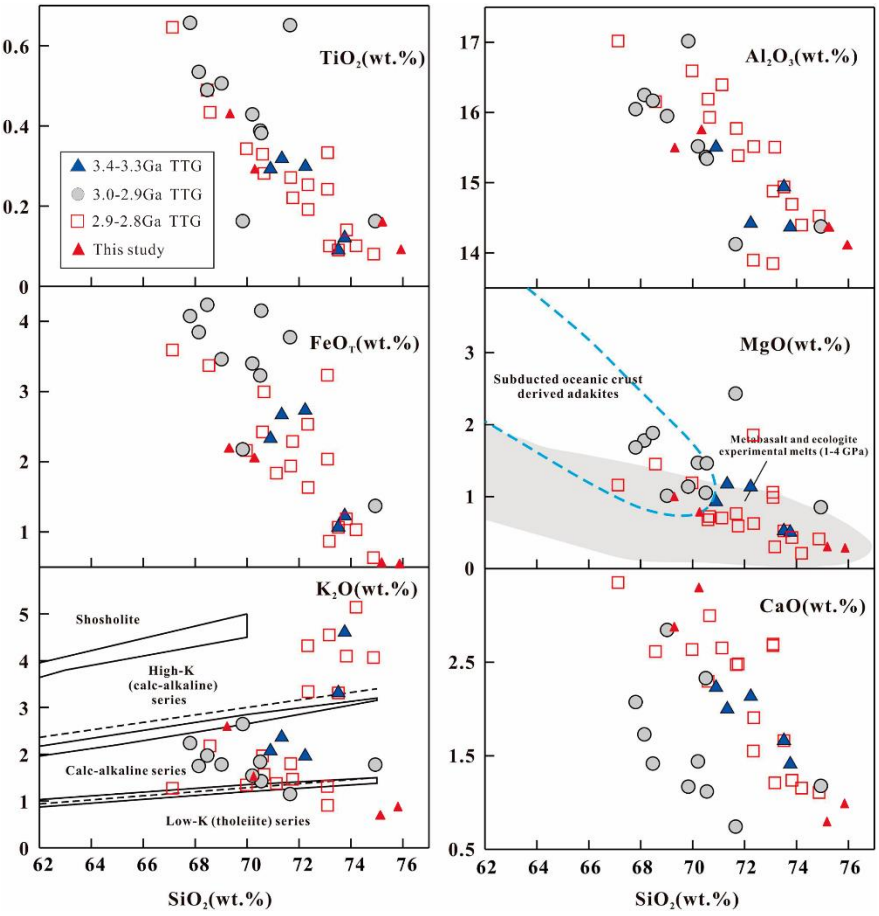

Figure 17. diagrams of gneissic granitoids from the Northern Kongling Terrane, showing SiO_2vs. (a) Na_2O, (b) K_2O, (c) Mg#, (d) MgO, (e) TFe_2O_3, and (f) CaO. Symbols: diamonds,TTGs; circles, biotite-granites; squares, two-mica granites; triangles, A-type granites. Data sources include this and previous studies (Gao et al., 1999, 2011; Xiong et al., 2009; Peng et al., 2012; Chen et al., 2013; Guo et al., 2014b; Li et al., 2014; Y.B. Wu's unpublished data).

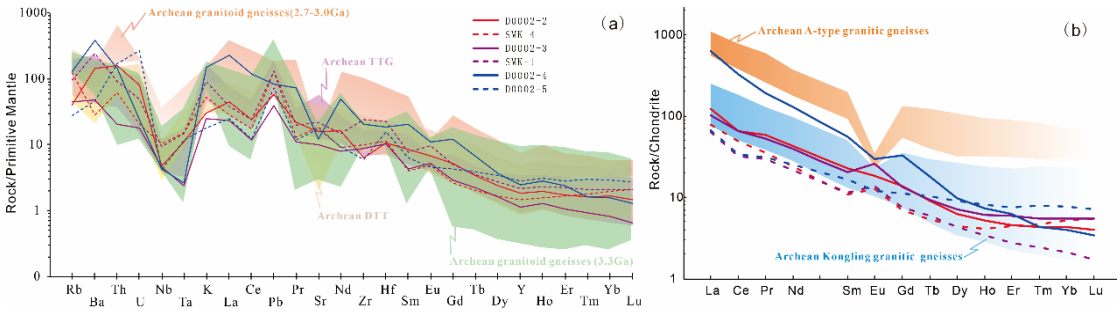

Figure 18. Primitive-mantle-normalized trace element distributions and Chondrite-normalized rare earth element patterns in the Archean TTG and granite dikes from the Kongling Terrane. Normalizing values are from McDonough and Sun (1989). The red and purple lines are for Kongling TTGs (D0002-2 and SMK-4 for tonalitic gneiss, and D0002-3 and SMK-1 for trondhjemite gneiss), and the blue lines are for granite dikes (D0002-4 and D0002-5). Data for the Archean granitoid gneisses, Archean TTG, and Archean DTT are from Gao et al. (2004b), Guo et al. (2014a), and Guo et al. (2015), respectively. for the Archean TTG and granite dikes from the Kongling Terrane.

Preprints (www.preprints.org) | NOT PEER-REVIEWED | Posted: 8 October 2019 doi:10.20944/preprints201910.0075.v1

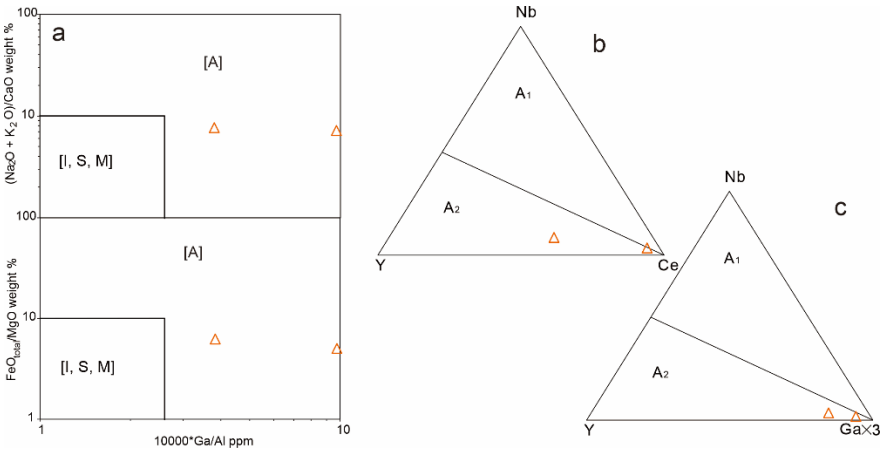

Figure 19. A-type granite discrimination diagrams. (a) $10^4 \times$ Ga/Al vs. FeO^T/MgO and (K_2O + Na_2O)/CaO discrimination diagrams of Whalen et al. (1987). [A] = A type granite, [I, S, M] = other granite types (I, S, and M-type granitoids). (b) Nb–Y–Ce and (c) Nb–Y–3Ga discrimination diagrams of Eby (1992).

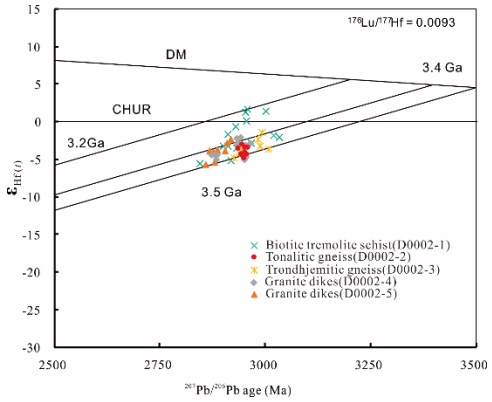

Figure 20. $\varepsilon_{Hf(t)}$ versus $^{207}Pb/^{206}Pb$ zircon age diagram for the biotite–tremolite schists, tonalitic gneisses, trondhjemitic gneisses, and granitic dikes.

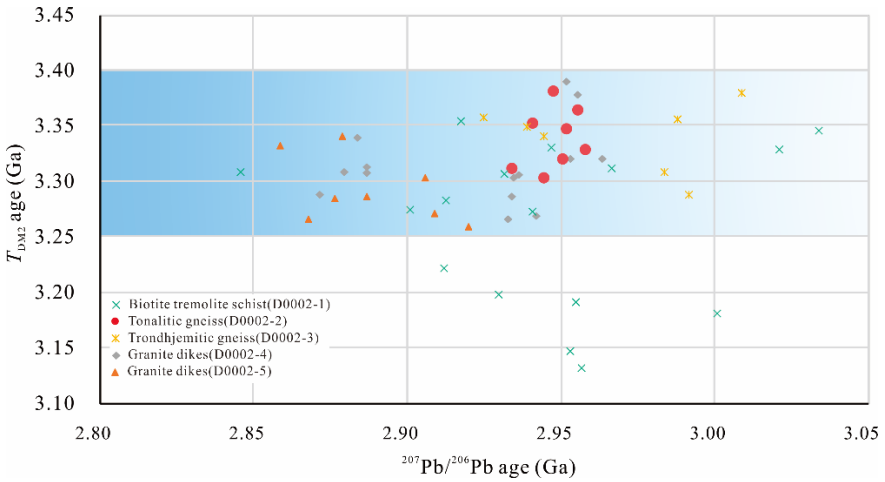

Figure 21. T_{DM2} age versus $^{207}Pb/^{206}Pb$ zircon age diagram for the biotite–tremolite schists, tonalitic gneisses, trondhjemitic gneisses, and granitic dikes.

Their trace element compositions are characterized by lower total REE values (53.69–105.08 ppm), enrichments in large ion lithophile elements (LILEs), depletions in high field strength elements (HFSEs) (e.g., Ti, Nb, Ta, and P), and low Cr (1.52–6.66 ppm) and Ni (2.87–

4.88 ppm) contents (Figure 17a). They show moderate amounts of heavy rare earth elements (HREEs) (e.g., 0.36–0.92 ppm Yb) and depletions in Eu (Eu/Eu*1.00–1.52) (Figure 17b; Table 6). These features make them similar to the rocks of the classic Archean TTG suite in this area (Gao et al., 1990; Guo et al., 2014a; Guo et al., 2015).

4.2.3. Granite Dikes

The two samples of granite gneisses from the dikes plot in the granite field on a K_2O vs. SiO_2 diagram with relatively high contents of SiO_2 (73.97 and 78.74 wt%), Na_2O (4.41 and 5.98 wt%), K_2O (4.28 and 0.52 wt%), and Al_2O_3 (13.11 and 12.85 wt%), and relatively low values of Mg# (30 and 55). The total contents of REEs are variable (443.68 and 62.35 ppm), but both samples show moderately negative Eu anomalies (Eu/ Eu* = 0.67–0.87; Figure 18b), notable depletions in Sr, P, and Eu, moderate depletions in Nb and Ta, enrichments in HFSEs (Th, U, Zr, and Hf), and alkali granite affinities (Figure 18a).

4.2.4. Zircon Hf-isotope

The zircon Lu–Hf isotopic data are given in Supplementary Data Table 7**,** and the $^{176}Hf/^{177}Hf(t)$ ratios were calculated back to their measured $^{207}Pb/^{206}Pb$ ages. The ε_{Hf} values were calculated with reference to a chondritic reservoir (CHUR). The values of $^{176}Lu/^{177}Hf$ and $^{176}Hf/^{177}Hf$ for the CHUR were 0.0336 and 0.282785, respectively [34]. A decay constant of 1.867×10^{-5} Ma^{-1} [35] was used for ^{176}Lu. The single-stage model age (T_{DM1}) was calculated relative to depleted mantle with present-day values of 0.28325 for $^{176}Hf/^{177}Hf$ and 0.0384 for $^{176}Lu/^{177}Hf$ [30]. The two-stage model age (T_{DM2}), interpreted as the crust formation age, was calculated by projecting the zircon $^{176}Hf/^{177}Hf(t)$ values back to the depleted-mantle model growth curve assuming a $^{176}Lu/^{177}Hf$ ratio of 0.0093 for the upper continental crust [36].

The Lu–Hf isotopes of 53 zircons from five samples were analyzed. As illustrated in Table 7, the $^{176}Hf/^{177}Hf(t)$ ratios of the concordant zircons show two distinct groups: the biotite–tremolite schists and others. The $^{176}Hf/^{177}Hf(t)$ ratios of the biotite–tremolite schists are higher than the ratios in the TTG gneisses and granitic dikes, ranging from 0.28077 to 0.28094 for the biotite–tremolite schists through 0.28075 to 0.28083 for the TTG gneisses and 0.28075 to 0.28085 for the granitic dikes. The $\varepsilon Hf(t)$ values of concordant zircons in the biotite–tremolite schists are close to 0 but range from 1.8 to –5.4 (Figure 20). The concordant zircons of the five samples have T_{DM2} ages ranging from 3.56 to 3.21 Ga (Figure 21).

5. DISCUSSION

5.1. Petrogenesis

5.1.1. Biotite Tremolite-schist

Although the Archean TTGs in the Kongling Terrane have been reported on and described by Guo, Gao [13] and [16], there has been relatively little research on Archean metabasites in the Yangtze Craton [37].

We noted in section of Whole-rock major and trace element compositions that all our Archean metabasite samples fall into the basaltic andesite and calc-alkaline series in the TAS volcanic rock classification. However, since the mobility of Si, Na, Ca, Rb, K, Sr, Ba, Fe, P, and Pb may have caused changes in the composition of volcanic rocks in Archean greenstone belts [38, 39], we selected instead Zr, Ti, Nb, and Y for classifying these rocks, but a similar result was obtained (Figure 15). We conclude, therefore, that the protoliths of the biotite–tremolite schists were calc-alkaline basaltic andesites, and their high ratios of K_2O/Na_2O (12.8) show that they were high-K island-arc volcanic rocks, and these rocks are generally considered to form by the partial melting of subducted oceanic crust.

Preprints (www.preprints.org) | NOT PEER-REVIEWED | Posted: 8 October 2019 doi:10.20944/preprints201910.0075.v1

5.1.2. TTG Magmatism

The ca. 2.9 Ga TTG gneisses are widespread in the North Kongling Terrane [7, 9, 15, 23, 40-42], and these felsic aluminous rocks are characterized by low Y (<18 ppm) and Yb (<1 ppm) contents as well as insignificant negative Eu anomalies, consistent with the definition of typical adakitic TTG rocks[43]. Typical suites of TTG and modern adakites were originally considered to result from the partial melting of a young and hot subducted oceanic crust [43, 44]. Subsequent studies have shown that such rocks can also be formed by (1) fractional crystallization of mafic minerals (mainly amphibole) in hydrous basaltic magmas under high pressure [45], (2) partial melting of adakitic melt-metasomatized lithospheric mantle [46], (3) partial melting of ancient thickened lower crust [47], (4) partial melting of a delaminated lower continental crust that underwent subsequent interaction with the surrounding asthenosphere [48], or (5) partial melting of pre-existing adakitic or TTG-like (mainly tonalitic) rocks [49].

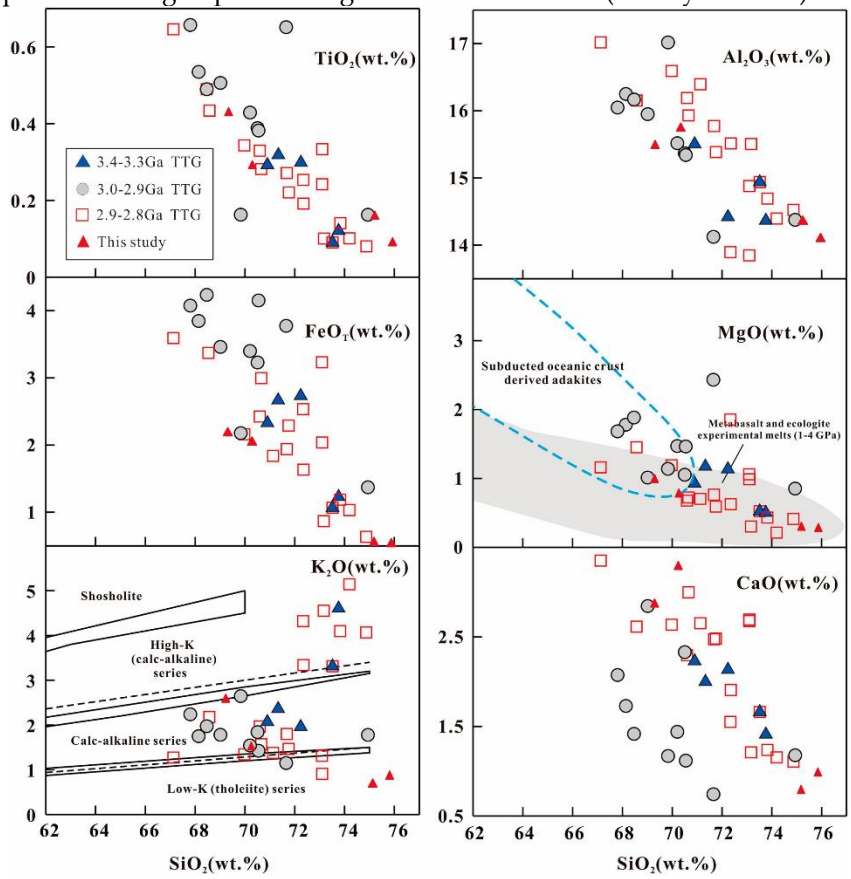

Figure 21. diagrams of gneissic granitoids from the Northern Kongling Terrane, showing SiO_2vs. (a) Na_2O, (b) K_2O, (c) Mg#, (d) MgO, (e) FeO_T, and (f) CaO. Symbols: diamonds,TTGs; circles, biotite-granites; squares, two-mica granites; triangles, A-type granites. Data sources include this and previous studies (Gao et al., 1999, 2011; Xiong et al., 2009; Peng et al., 2012; Chen et al., 2013; Guo et al., 2014b; Li et al., 2014; Y.B. Wu's unpublished data).

The major element compositions of the TTG samples fall close to the field of partial melts from low-K mafic rocks as the 3.3Ga-2.9Ga TTGs [16](Figure 22). They show weak Eu and Sr anomalies, low contents of HREEs (e.g., 0.36–0.92 ppm Yb), and moderate La_N/Yb_N ratios (15–29), indicating an eclogite-facies source region [50](Figure 18). The ca. 2.9 Ga TTG gneisses also exhibit variable values of $Mg^{\#}$ (41–47) and variable contents of Cr (1.7–12.32 ppm) and Ni (2.87–8.41 ppm), which could be explained by interactions of the TTG melts with mantle rocks, possibly in a subduction zone [51-53]. Mafic xenoliths or veins hosted in the ca. 2.9 Ga TTGs [37, 41, 54] have chemical affinities to typical island arc basalts, which lends support to an origin

Preprints (www.preprints.org) | NOT PEER-REVIEWED | Posted: 8 October 2019 doi:10.20944/preprints201910.0075.v1

in a subduction setting. The possible tectonic settings include an oceanic island arc setting and a continental arc setting[41].

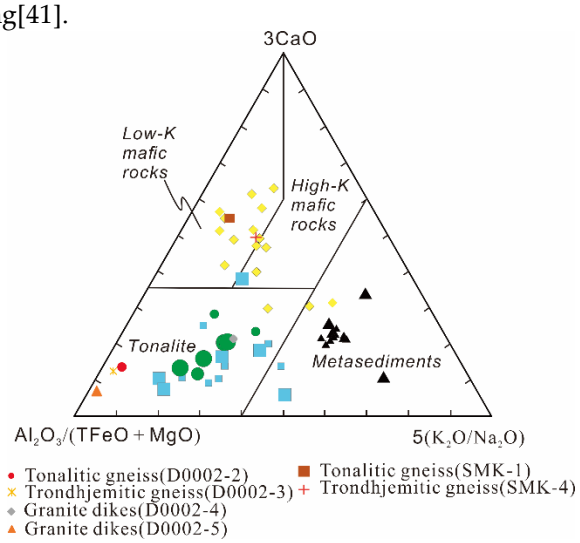

Figure 22. Ternary diagram of Al_2O_3/(TFeO + MgO) vs. 3CaO vs. 5(K_2O/Na_2O) (after Laurent et al., 2014). The different fields represent the compositions of melts derived from a range of potential sources (tonalites, metasediments, low- and high-K mafic rocks), determined by the major-element compositions of partial melts in experimental studies (see references in Laurent et al., 2014). Symbols: diamonds = TTGs, circles = biotite granites, squares = two-mica granites, triangles = A-type granites. Data sources include this and previous studies[7, 13, 15, 19, 41, 55, 56] and unpublished data of Wu Y.B..

In oceanic island arcs, both the subducting and the overriding plates are juvenile oceanic crust. Thus, the granitoids produced in such an environment would exhibit radiogenic Hf isotopic compositions, with depleted mantle-like εHf(t) values [57]. This is in conflict with the non-radiogenic nature of the zircons in the ca. 2.9 Ga TTG rocks, which exhibit a wide range of εHf(t) values, but with predominantly subchondritic values (Figure 20 and Figure 21). The >3.2 Ga T_{DM2} ages and the small number of 3.2 Ga inherited zircons in the 3.0–2.9 Ga TTG gneisses [23] indicate a vital role was played by an ancient crystalline basement in the genesis of these rocks, which actually fits a continental arc setting. In continental arcs, due to the melting and/or contamination of the overriding thick ancient continental crust above the subduction zone, the granitoid magmas therein are commonly imprinted by less radiogenic Hf features and characterized by lower εHf(t) values [58-60]. Therefore, the tectonic environment of the Kongling Terrane during the period 3.0–2.9 Ga may have been like a modern continental arc, indicating that plate tectonics in the Yangtze Craton commenced before 2.9 Ga.

Fourteen zircons from trondhjemitic gneisses containing core–rim structures yielded an upper intercept age of 3.00 Ga (Figure 18a and Table 6), and they might represent zircons inherited from their parental rocks. The Lu–Hf isotopes also provide the same εHf(t) values and single- and two-stage model ages as the metamorphic zircon cores of the biotite–tremolite schists. All this evidence seems to be generally consistent with the proposal that the TTGs were derived from the partial melting of juvenile crust in the same subduction setting that produced the parental magmas of the metamorphosed basaltic andesite from subducted oceanic crust. These parental magmas might indeed have contributed to the juvenile crust through a process of underplating.

5.1.3. Alkali Granite Dikes

As discussed in section of whole-rock major and trace element compositions, the later dikes show affinities to typical alkali granites. Our two samples of alkali granite plot uniformly in the A_2 field on the A-type granite discrimination diagrams of Eby [61] (Figure 19), which

relates to a post-collisional extensional tectonic setting [62] on an active continental margin, and the melting of continental crust or an underplated mafic crust.

Zircons from the dike rocks show two groups of ages, and the 2.91–2.94 Ga ages of the larger group are essentially the same as the emplacement ages of the TTG gneisses, discussed above. In addition, their similar εHf(t) values and single- and two-stage model ages indicate that both the TTGs and the dikes may be the outcomes of a multistage process of partial melting of the biotite–tremolite schists.

5.2. Tectonic implications

The recently discovered biotite–tremolite schists in the Kongling Terrane, the subject of this paper, are among the oldest rocks of the Yangtze Craton. Consequently, understanding their genesis and evolution is key to understanding the initiation of plate tectonics in South China.

Two groups of zircon $^{206}Pb/^{207}Pb$ ages were obtained from the zircons with core–rim structures of the biotite–tremolite schists, with the cores giving the older age of 3.00 Ga. Although the Th/U ratios in the cores are slightly higher than in the rims, their images are light-colored with flower shapes or cloud rings, which are characteristics of recrystallized zircons (Figure 4). The 3.00 Ga ages of the zircon cores can probably be treated as a record of early metamorphic/magmatic events. The low contents of U in the zircons might result in the metamorphic ages still falling on or near the concordant curve.

The Lu–Hf isotope data also indicate that the biotite–tremolite schists formed at around 3.00 Ga, which is the same age as shown by the metamorphic zircon cores. The single- and two-stage model ages of hafnium are 3.26 Ga and 3.39 Ga, respectively, and these ages are within error of the ages of the metamorphic zircon cores. The zircons have relatively high negative εHf(t) values ranging from –3.5 up to 1.7 (average –1.9), and this seems to be consistent with the idea that the parental magmas of the metamorphosed basaltic andesites were derived from the partial melting of juvenile crust with small amounts of mantle components added in a subduction zone setting.

Apart from the magmatic events, ages of 2.93 Ga were obtained from both cores and rims. These 2.93 Ga zircons cores show dark CL images and low Th/U ratios (<0.1), indicating that the grains underwent a metamorphic recrystallization in the presence of fluids. The rims of the zircons show uniform structures in the CL images, and they have low Th/U ratios (<0.1). As the zircons with higher U contents display greater Pb loss, the data from the analytical spots fall on the discordia curve with a 2.93 Ga upper intercept age. These two important thermal events can also be observed in the age data for the zircons from the Dongchonghe TTG rocks (D0002-2 and D0002-3), which are interpreted to be the same as other tectonothermal events recorded by zircons, as described by Gao et al. (2011), Qiu et al. (2000), and Zhang et al. (2006a).

The 3.3–3.0 Ga metamorphic/magmatic events might be related to the subduction of oceanic crust that produced the trondhjemites and the high-K calc-alkaline island-arc basaltic andesites. The 2.93–2.91 Ga ages would be related to the first metamorphic event that occurred when the TTG granites and tholeiitic basaltic rock enclaves were transformed into TTG gneisses and amphibolite enclaves, respectively, while the ~2.87 Ga alkaline magmatism was related to a regional post-orogenic extensional environment. Guo, Wu [16] pointed out that the granitoid magmatism changed from TTG- to granite-dominated after 2.8 Ga, and this change may reflect a transition from subduction to collision-related events.

Taking into account the several tectonic/magmatic thermal events that have been described in the previous literature at 2.75–2.70 Ga and 2.6–2.5 Ga [54], and 2.1–1.9 Ga [12, 17, 63-65], our latest data show that the Yangtze continental nucleus underwent at least five widespread tectonic/magmatic thermal events during the Paleoproterozoic and the Mesoarchean.

 doi:10.20944/preprints201910.0075.v1

6. CONCLUSIONS

1) The ages of the early cores of zircons from the biotite–tremolite schist enclaves hosted by the TTG gneisses in the Kongling high-grade metamorphic terrane of the Yangtze Craton, China, are similar to the metamorphic recrystallization ages and model ages indicated by Hafnium isotopes (ca. 3.00 Ga), which suggests that the basaltic protoliths of these schists were formed before or close to 3.00 Ga. The data indicate that these schists represent the metamorphosed basaltic igneous rocks that formed the basal part of a Mesoarchean granite–greenstone belt.

2) The host TTG gneisses were derived from the partial melting of subducted oceanic crust, which is consistent with the proposal that the early metamorphic/tectonic thermal events in the Yangtze continental core record the initiation of global plate tectonics at 3.00 Ga.

Author Contributions: Conceptualization, Wenxiao Zhou and Yunxu Wei; Data curation, Wenxiao Zhou and Haiquan Li; Formal analysis, Wenxiao Zhou; Project administration, Yunxu Wei; Resources, Zhengxiang Hu, Xianxiao Huang and Xiaoming Zhao; Writing – original draft, Wenxiao Zhou; Writing – review & editing, Wenxiao Zhou.

Funding: This study is supported by the National Natural Science Foundation of China (No. 41703024) and the work items of China Geological Survey (No. DD20190374, DD20160029, 12120113061700).

Conflicts of Interest: The authors declare no conflict of interest.

References

1. Hacker, B.R., et al., *U/Pb zircon ages constrain the architecture of the ultrahigh-pressure Qinling–Dabie Orogen, China.* Earth and Planetary Science Letters, 1998. **161**(1): p. 215-230.
2. Li, S., et al., *Collision of the North China and Yangtse Blocks and formation of coesite-bearing eclogites: Timing and processes ☆.* Chemical Geology, 1993. **109**(1-4): p. 89-111.
3. Zhang, S.-B. and Y.-F. Zheng, *Formation and evolution of Precambrian continental lithosphere in South China.* Gondwana Research, 2013. **23**(4): p. 1241-1260.
4. Wu, Y.B., et al., *Zircon U-Pb age and trace element evidence for Paleoproterozoic granulite-facies metamorphism and Archean crustal rocks in the Dabie Orogen.* Lithos, 2008. **101**(3-4): p. 308-322.
5. Wu, F.-Y., et al., *Zircon U–Pb and Hf isotopic constraints on the Early Archean crustal evolution in Anshan of the North China Craton.* Precambrian Research, 2008. **167**(3-4): p. 339-362.
6. Song, B., et al., *3800 to 2500 Ma crustal evolution in the Anshan area of Liaoning Province, northeastern China.* Precambrian Research, 1996. **78**(79): p. 79-94.
7. Gao, S., et al., *Age and growth of the Archean Kongling terrain, South China, with emphasis on 3.3 Ga granitoid gneisses.* Geochimica Et Cosmochimica Acta Supplement, 2011. **72**(12): p. 153-182.
8. Jiao, W.F., et al., *The oldest basement rock in the Yangtze Craton revealed by zircon U-Pb age and Hf isotope composition.* Science In China Series D-Earth Sciences, 2009. **52**(9): p. 1393-1399.
9. Qiu, Y., et al., *First evidence of >3.2 Ga continental crust in the Yangtze craton of south China and its implications for Archean crustal evolution and Phanerozoic tectonics.* Geology, 2000. **28**(1): p. 11.
10. Zhang, S.B., et al., *Zircon U-Pb age and Hf isotope evidence for 3.8 Ga crustal remnant and episodic reworking of Archean crust in South China.* Earth And Planetary Science Letters, 2006. **252**(1-2): p. 56-71.
11. Qiu, X.-F., et al., *Evolution of the Archean continental crust in the nucleus of the Yangtze block: Evidence from geochemistry of 3.0 Ga TTG gneisses in the Kongling high-grade metamorphic terrane, South China.* Journal of Asian Earth Sciences, 2018. **154**: p. 149-161.
12. Ling, W., et al., *Sm-Nd isotope geochronology of the Qiling complex in the Huangling area of the Yangtze Craton.* Chinese Science Bulletin, 1998. **43**(1): p. 86.
13. Guo, J.L., et al., *3.45 Ga granitic gneisses from the Yangtze Craton, South China: Implications for Early Archean crustal growth.* Precambrian Research, 2014. **242**: p. 82-95.
14. Liu, X., et al., *Precambrian crustal growth of Yangtze Craton as revealed by detrital zircon studies.* American Journal of Science, 2008. **308**(4): p. 421-468.
15. Chen, K., et al., *2.6-2.7 Ga crustal growth in Yangtze craton, South China.* Precambrian Research, 2013. **224**: p. 472-490.
16. Guo, J.L., et al., *Episodic Paleoarchean-Paleoproterozoic (3.3-2.0 Ga) granitoid magmatism in Yangtze Craton, South China: Implications for late Archean tectonics.* Precambrian Research, 2015. **270**: p. 246-266.
17. Zhang, S.B., et al., *Zircon U-Pb age and Hf-O isotope evidence for Paleoproterozoic metamorphic event in South China.* Precambrian Research, 2006. **151**(3): p. 265-288.
18. Li, Z., et al., *Grenvillian continental collision in south China: New SHRIMP U-Pb zircon results and implications for the configuration of Rodinia.* Geology, 2002. **30**(2): p. 163-166.

19. Gao, S., et al., *Contrasting geochemical and Sm-Nd isotopic compositions of Archean metasediments from the Kongling high-grade terrain of the Yangtze craton: Evidence for cratonic evolution and redistribution of REE during crustal anatexis.* Geochimica Et Cosmochimica Acta, 1999. **63**(13-14): p. 2071-2088.
20. Ling, W., et al., *Neoproterozoic magmatic events within the Yangtze continental interior and along its northern margin and their tectonic implication: constraint from the ELA-ICPMS U-Pb geochronogy of zicrons from the Huangling and Hannan complexes*, in *Acta Petrologica Sinica*. 2006. p. 387-396.
21. Wei, Y., et al., *SHRIMP zircon U-Pb ages and geochemical characteristics of the neoproterozoic granitoids in the Huangling anticline and its tectonic setting.* Journal of Earth Science, 2012. **23**(5): p. 659-676.
22. Zhang, S.-B., et al., *Neoproterozoic anatexis of Archean lithosphere: Geochemical evidence from felsic to mafic intrusions at Xiaofeng in the Yangtze Gorge, South China.* Precambrian Research, 2008. **163**(3-4): p. 210-238.
23. Zhang, S.B., et al., *Zircon isotope evidence for ⩾3.5Ga continental crust in the Yangtze craton of China.* Precambrian Research, 2006. **146**(1): p. 16-34.
24. Ballard, J.R., et al., *Two ages of porphyry intrusion resolved for the super-giant Chuquicamata copper deposit of northern Chile by ELA-ICP-MS and SHRIMP.* Geology, 2001. **29**(5): p. 383-386.
25. Yuan, H., et al., *Accurate U-Pb age and trace element determinations of zircon by laser ablation-inductively coupled plasma-mass spectrometry.* Geostandards and Geoanalytical Research, 2004. **28**(3): p. 353-370.
26. Andersen, T., *Correction of common lead in U–Pb analyses that do not report 204Pb.* Chemical geology, 2002. **192**(1-2): p. 59-79.
27. Ludwig, K.R., *Isoplot 3.00: A geochronological toolkit for Microsoft Excel.* Berkeley Geochronology Center Special Publication, 2003. **4**: p. 70.
28. Hu, Z., et al., *Improved in situ Hf isotope ratio analysis of zircon using newly designed X skimmer cone and jet sample cone in combination with the addition of nitrogen by laser ablation multiple collector ICP-MS.* Journal of Analytical Atomic Spectrometry, 2012. **27**(9): p. 1391-1399.
29. Hu, Z., et al., *A "wire" signal smoothing device for laser ablation inductively coupled plasma mass spectrometry analysis.* Spectrochimica Acta Part B: Atomic Spectroscopy, 2012. **78**: p. 50-57.
30. Griffin, W.L., et al., *Zircon chemistry and magma mixing, SE China: in-situ analysis of Hf isotopes, Tonglu and Pingtan igneous complexes.* Lithos, 2002. **61**(3-4): p. 237-269.
31. O'connor, J., *A classification for quartz-rich igneous rocks based on feldspar ratios.* US Geological Survey Professional Paper B, 1965. **525**: p. 79-84.
32. Frost, B.R., et al., *A geochemical classification for granitic rocks.* Journal of petrology, 2001. **42**(11): p. 2033-2048.
33. Maniar, P.D. and P.M. Piccoli, *Tectonic discrimination of granitoids.* Geological society of America bulletin, 1989. **101**(5): p. 635-643.
34. Bouvier, A., J.D. Vervoort, and P.J. Patchett, *The Lu–Hf and Sm–Nd isotopic composition of CHUR: constraints from unequilibrated chondrites and implications for the bulk composition of terrestrial planets.* Earth and Planetary Science Letters, 2008. **273**(1-2): p. 48-57.
35. Söderlund, U., et al., *The 176Lu decay constant determined by Lu–Hf and U–Pb isotope systematics of Precambrian mafic intrusions.* Earth and Planetary Science Letters, 2004. **219**(3-4): p. 311-324.

36. Vervoort, J.D. and P.J. Patchett, *Behavior of hafnium and neodymium isotopes in the crust: constraints from Precambrian crustally derived granites.* Geochimica et Cosmochimica Acta, 1996. **60**(19): p. 3717-3733.
37. Wei, J.Q. and M.M. Jing, *Chronology and geochemistry of amphibolites from the Kongling complex.* Chinese Journal of Geology, 2013. **48**(4): p. 970-983.
38. Polat, A. and A. Hofmann, *Alteration and geochemical patterns in the 3.7–3.8 Ga Isua greenstone belt, West Greenland.* Precambrian Research, 2003. **126**(3-4): p. 197-218.
39. Polat, A., A. Hofmann, and M.T. Rosing, *Boninite-like volcanic rocks in the 3.7–3.8 Ga Isua greenstone belt, West Greenland: geochemical evidence for intra-oceanic subduction zone processes in the early Earth.* Chemical geology, 2002. **184**(3-4): p. 231-254.
40. Guo, J.-L., et al., *Episodic Paleoarchean-Paleoproterozoic (3.3–2.0 Ga) granitoid magmatism in Yangtze Craton, South China: Implications for late Archean tectonics.* Precambrian Research, 2015. **270**: p. 246-266.
41. Li, L., et al., *Geochronology and geochemistry of igneous rocks from the Kongling terrane: Implications for Mesoarchean to Paleoproterozoic crustal evolution of the Yangtze Block.* Precambrian Research, 2014. **255**: p. 30-47.
42. Zheng, J., et al., *Widespread Archean basement beneath the Yangtze craton.* Geology, 2006. **34**(6): p. 417-420.
43. Defant, M.J. and M.S. Drummond, *Derivation of some modern arc magmas by melting of young subducted lithosphere.* Nature, 1990. **347**(6294): p. 662.
44. Barker, F. and J.G. Arth, *Generation of trondhjemitic-tonalitic liquids and Archean bimodal trondhjemite-basalt suites.* Geology, 1976. **4**(10): p. 596-600.
45. Castillo, P.R., *An overview of adakite petrogenesis.* Chinese science bulletin, 2006. **51**(3): p. 257-268.
46. Gao, Y., et al., *Adakitic rocks from slab melt-modified mantle sources in the continental collision zone of southern Tibet.* Lithos, 2010. **119**(3-4): p. 651-663.
47. Chung, S.-L., et al., *Adakites from continental collision zones: melting of thickened lower crust beneath southern Tibet.* Geology, 2003. **31**(11): p. 1021-1024.
48. Gao, S., et al., *Recycling lower continental crust in the North China craton.* Nature, 2004. **432**(7019): p. 892-7.
49. Moyen, J.-F., *High Sr/Y and La/Yb ratios: the meaning of the "adakitic signature".* Lithos, 2009. **112**(3-4): p. 556-574.
50. Moyen, J.-F., *The composite Archaean grey gneisses: petrological significance, and evidence for a non-unique tectonic setting for Archaean crustal growth.* Lithos, 2011. **123**(1-4): p. 21-36.
51. Martin, H. and J.-F. Moyen, *Secular changes in tonalite-trondhjemite-granodiorite composition as markers of the progressive cooling of Earth.* Geology, 2002. **30**(4): p. 319-322.
52. Martin, H., et al., *An overview of adakite, tonalite–trondhjemite–granodiorite (TTG), and sanukitoid: relationships and some implications for crustal evolution.* Lithos, 2005. **79**(1-2): p. 1-24.
53. Moyen, J.-F. and H. Martin, *Forty years of TTG research.* Lithos, 2012. **148**: p. 312-336.
54. Wei, J. and J. Wang, *Zircon age and Hf isotope compositions of amphibolite enclaves from the Kongling complex.* Geol. J. China Univ., 2012. **18**(4): p. 589-600.

665 55. Peng, M., et al., *Geochemistry, zircon U–Pb age and Hf isotope compositions of Paleoproterozoic*
666 *aluminous A-type granites from the Kongling terrain, Yangtze Block: Constraints on petrogenesis*
667 *and geologic implications.* Gondwana Research, 2012. **22**(1): p. 140-151.
668 56. Xiong, Q., et al., *Zircon U-Pb age and Hf isotope of Quanyishang A-type granite in Yichang:*
669 *signification for the Yangtze continental cratonization in Paleoproterozoic.* Chinese Science
670 Bulletin, 2009. **54**(3): p. 436-446.
671 57. Schaltegger, U., et al., *Multiple mantle sources during island arc magmatism: U–Pb and Hf isotopic*
672 *evidence from the Kohistan arc complex, Pakistan.* Terra Nova, 2002. **14**(6): p. 461-468.
673 58. Ducea, M.N., J.B. Saleeby, and G. Bergantz, *The Architecture, Chemistry, and Evolution of*
674 *Continental Magmatic Arcs.* Annual Review of Earth and Planetary Sciences, 2015. **43**(1): p. 299-
675 331.
676 59. Jones, R.E., et al., *Geodynamic controls on the contamination of Cenozoic arc magmas in the*
677 *southern Central Andes: Insights from the O and Hf isotopic composition of zircon.* Geochimica et
678 Cosmochimica Acta, 2015. **164**: p. 386-402.
679 60. Li, Z.-X., et al., *Magmatic switch-on and switch-off along the South China continental margin since*
680 *the Permian: Transition from an Andean-type to a Western Pacific-type plate boundary.* 2012. **532**:
681 p. 271-290.
682 61. Eby, G.N., *Chemical subdivision of the A-type granitoids: Petrogenetic and tectonic implications.*
683 Geology, 1992. **20**(7): p. 641-644.
684 62. Bonin, B., *A-type granites and related rocks: Evolution of a concept, problems and prospects.*
685 Lithos, 2007. **97**(1-2): p. 1-29.
686 63. Han, Q.S., et al., *A ca.2.1 Ga Andean-type margin built on metasomatized lithosphere in the*
687 *northern Yangtze craton, China: Evidence from high-Mg basalts and andesites.* Precambrian
688 Research, 2017. **309**: p. 309-324.
689 64. Ling, W.L. and S. Gao, *The tectonic thermal events and the evolution in the late Paleoproterozoic*
690 *of the Yangtze craton in the Yangtze.* Chinese Science Bulletin, 2000. **45**(21): p. 2343-2347.
691 65. Peng, S., et al., *The discovery of Paleoproterozoic ophiolitic melange in the northern part of the*
692 *Huangling Dome of the Yangtze Craton.* Journal of Earth Science, 2016. **41**(12): p. 2117-2118.
693